iScience

CellPress
OPEN ACCESS

Article

Drosophila PTPMT1 Has a Function in Tracheal Air Filling

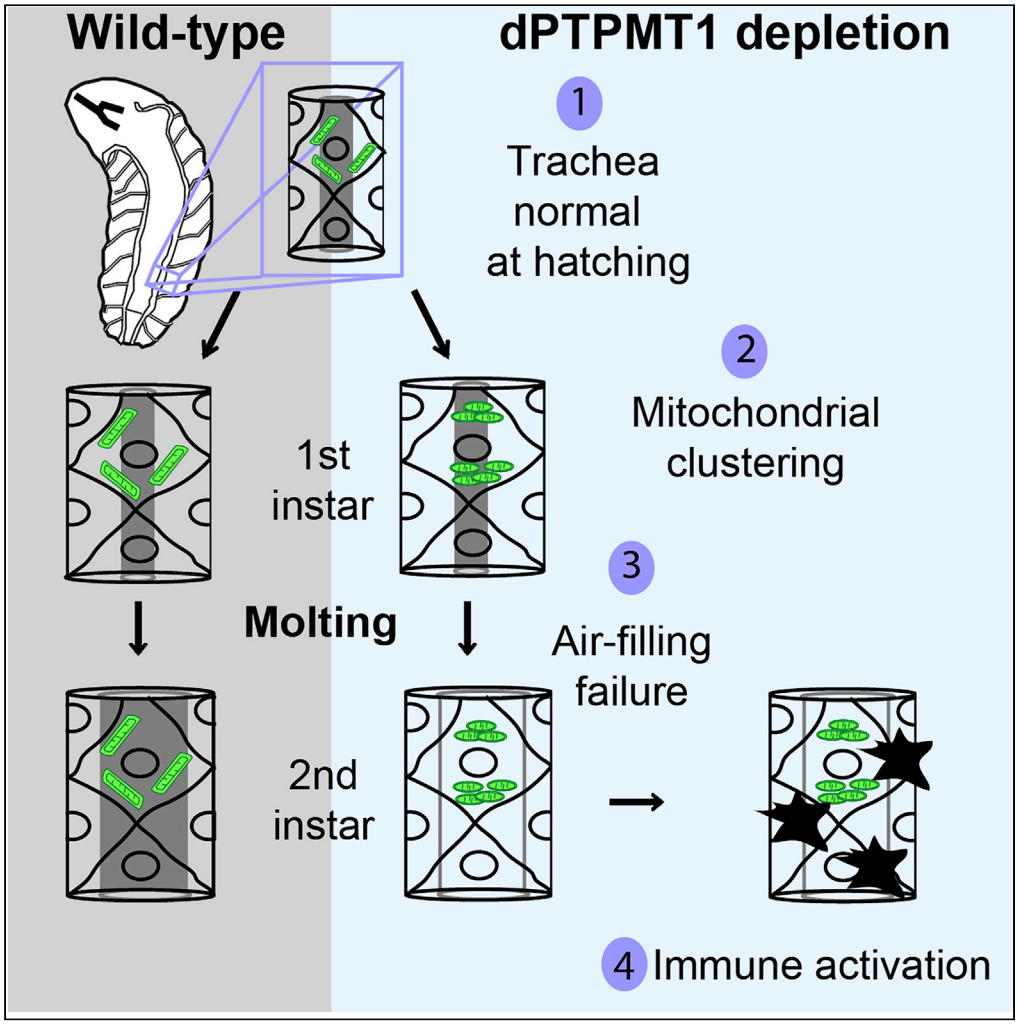

Amanda M. Papakyrikos, Min Joo Kim, Xinnan Wang

xinnanw@stanford.edu

HIGHLIGHTS

A *Drosophila* model of PTPMT1 depletion is generated

PTPMT1 mutants show impairments in tracheal air filling

Mitochondria aggregate within the tracheal epithelial cells prior to air-filling failure

Depletion of the cardiolipin pathway components does not mimic *PTPMT1* deficiency

Papakyrikos et al., iScience *23*, 101285
July 24, 2020
https://doi.org/10.1016/j.isci.2020.101285

iScience

CellPress
OPEN ACCESS

Article

Drosophila PTPMT1 Has a Function in Tracheal Air Filling

Amanda M. Papakyrikos,[1,2] Min Joo Kim,[1] and Xinnan Wang[1,3,*]

SUMMARY

The fly trachea is the equivalent of the mammalian lung and is a useful model for human respiratory diseases. However, little is known about the molecular mechanisms underlying tracheal air filling during larval development. In this study, we discover that PTPMT1 has a function in tracheal air filling. PTPMT1 is a widely conserved, ubiquitously expressed mitochondrial phosphatase. To reveal PTPMT1's functions in genetically tractable invertebrates and whether those functions are tissue specific, we generate a *Drosophila* model of PTPMT1 depletion. We find that fly *PTPMT1* mutants show impairments in tracheal air filling and subsequent activation of innate immune responses. On a cellular level, these defects are preceded by aggregation of mitochondria within the tracheal epithelial cells. Our work demonstrates a cell-type-specific role for PTPMT1 in fly tracheal epithelial cells to support air filling and to prevent immune activation. The establishment of this model will facilitate exploration of PTPMT1's physiological functions *in vivo*.

INTRODUCTION

The fly respiratory system (i.e., the trachea) is the equivalent of the mammalian lung with similarities in development and immunity, which make it a useful model for numerous human respiratory diseases (Bergman et al., 2017). The tracheal system consists of a network of air-filled epithelial tubes. These tubes contain a cuticular lining that provides structural support, through ridges known as taenidia. As the larva grows the trachea must also grow to match the increased oxygen demand of the tissue. During molting the old cuticular lining separates from the tracheal epithelium, and what is presumed to be molting fluid fills the space between the old and new lining. The old lining collapses and is removed from the trachea, followed immediately by filling of the trachea with air and removal of molting fluid (Park et al., 2002). However, little is known about the molecular mechanisms underlying larval tracheal air filling.

The trachea is open to the environment and thus vulnerable to infection. Tracheal epithelial cells have a number of innate defenses including the expression of antimicrobial peptides (AMPs) (Tzou et al., 2000; Wagner et al., 2009; Bergman et al., 2017) and melanization, an arthropod-specific response to wounds or infections (Tang et al., 2008). The production of melanin is catalyzed by prophenoloxidases (PPOs), zymogens that are activated by serine protease cascades (Tang et al., 2006; Dudzic et al., 2019). Outside the trachea, melanization is typically mediated by specialized immune cells known as crystal cells, which can be triggered to release PPOs into the hemolymph (Tang, 2009).

Mitochondria are extremely multifaceted organelles with roles in metabolism, apoptosis, cell signaling, and more. Reversible phosphorylation is one mechanism by which mitochondrial activities are regulated (Pagliarini and Dixon, 2006). Protein-tyrosine-phosphatase localized to the mitochondrion 1 (PTPMT1) is a phosphatase that resides on the inner mitochondrial membrane, where it regulates mitochondrial functions through its phosphatase activity (Pagliarini et al., 2004, 2005). Studies from vertebrate systems have shown that PTPMT1 controls pyruvate importation and utilization in the mitochondria through regulation of phosphatidylinositol phosphate (PIP) levels, modulates crista structure and respiratory chain function through the synthesis of cardiolipin (CL)—the hallmark phospholipid of the mitochondria (Zhang et al., 2011; Xiao et al., 2011; Teh et al., 2013), and regulates the tricarboxylic acid (TCA) cycle through succinate dehydrogenase (Nath et al., 2015). Loss of *PTPMT1* in a variety of mammalian cell types results in decreased mitochondrial respiration and increased glycolysis. These metabolic changes have drastic impacts on stem cells and cancer cells, but not on other cell types, demonstrating that the functional consequences of

[1]Department of Neurosurgery, Stanford University School of Medicine, Stanford, CA 94305, USA

[2]Graduate Program in Developmental Biology, Stanford University School of Medicine, Stanford, CA 94305, USA

[3]Lead Contact

*Correspondence: xinnanw@stanford.edu

https://doi.org/10.1016/j.isci.2020.101285

PTPMT1 depletion are highly cell-type-specific (Pagliarini et al., 2005; Shen et al., 2011; Zhang et al., 2011; Niemi et al., 2013; Yu et al., 2013; Zheng et al., 2018). Although PTPMT1 is broadly expressed and highly conserved among species (Pagliarini et al., 2004, 2005; Shen et al., 2011; Teh et al., 2013), to date, it has only been examined in a narrow number of tissues and cell types and predominately in vertebrates, limiting our understanding of PTPMT1's distinct cell-type-specific roles *in vivo*. *Drosophila melanogaster* is an unparalleled genetic model for studying tracheal biology and gene function, with methods for the rapid generation of mutants as well as expansive collections of existing mutants and RNA interference (RNAi) lines. Here, we examine the physiological functions of *PTPMT1* in *Drosophila* and report a role for PTPMT1 in fly tracheal epithelial cells.

RESULTS

dPTPMT1 Is an Essential Gene in *Drosophila*

To study the function of *Drosophila* PTPMT1 (dPTPMT1), we employed CRISPR-CAS9 to create a defined deletion in *dPTPMT1* that would remove most of its coding sequence (Gratz et al., 2013, 2015) (Figure S1A). We failed to isolate the intended deletion but were able to obtain three independent lines with small deletions in the regions targeted by our gRNAs: $dPTPMT1^{mut1}$ (c.487delA), $dPTPMT1^{mut2}$ (c.479_489delCGGATGGACTC), and $dPTPMT1^{mut3}$ (c.12 + 82delT and c487delA) (Figures 1A, S1B, and S1C). All three lines were homozygous lethal and also lethal over two deficiency lines covering *dPTPMT1* (*Df(3R)BSC490* and *Df(3R)Exel9013*). The failure to complement indicates that lethality is likely caused by mutations in *dPTPMT1*. In all lines, both as homozygotes and transheterozygotes (over *Df(3R)BSC490*), third instar larvae were present, albeit at reduced frequencies, likely due to the increased early lethality (Figure 1B). None of these larval escapers were able to undergo pupariation and survive to adulthood (Figure 1C). We collected age-synchronized embryos (3 h after egg laying–AEL) and examined viability 24 h AEL. We found approximately 80% of first instar larvae of $dPTPMT1^{mut1}$ that hatched died soon after (Figure 1B). The lethality rates were comparable between $dPTPMT1^{mut1}$ homozygotes and transheterozygotes. These results suggest that $dPTPMT1^{mut1}$represents a null allele or strong hypomorph.

To complement the CRISPR mutants, we obtained three *UAS-dPTPMT1* RNAi lines from the Vienna *Drosophila* RNAi Center and the *Drosophila* Transgenic RNAi Project collections (Dietzl et al., 2007; Perkins et al., 2015). All three *UAS-dPTPMT1* RNAi insertions are at independent genomic locations. RNAi 1 and 2 target the same region within the third exon of *dPTPMT1*, whereas RNAi 3 targets the fourth exon of *dPTPMT1*, allowing us to control for off-target effects (Figure 1A). Ubiquitous *dPTPMT1* RNAi with the driver *Act5C-GAL4* reduced *dPTPMT1* transcripts to below 20% of wild-type levels for all three lines, as detected by quantitative real-time PCR (qPCR) (Figure S1D). *dPTPMT1* RNAi 1 and 3 were pupal lethal (Figure 1D). RNAi 2 allowed adult survivors but with a significant decrease in viability compared with wild-type controls (Figure 1D). Given the conservation in protein sequence between PTPMT1 and PTEN's catalytic regions (Pagliarini et al., 2004), we also verified that *dPTPMT1* RNAi did not affect fly *PTEN* (*dPten*) transcript levels by qPCR (Figure S1E).

To study the structure-function relationship of dPTPMT1 *in vivo*, we generated *UAS-dPTPMT1* transgenic fly lines, including wild-type (WT) *dPTPMT1*, catalytic-dead (CD; with a C141S mutation) *dPTPMT1*, and *dPTPMT1* with a deletion of its putative mitochondrial targeting sequence (ΔMTS; removing amino acids 1–31) (Pagliarini et al., 2005). All transgenes were inserted into the same genomic region using the PhiC31 integrase-mediated transgenesis system (Markstein et al., 2008). To test the functional conservation of PTPMT1 between flies and humans, we also generated *UAS-human PTPMT1 (hPTPMT1)* and *UAS-hPTPMT1-CD* (C132S) (Zhang et al., 2011). Because we were unable to generate an antibody or identify a commercially available antibody that recognized dPTPMT1, we tagged all transgenes with *3×FLAG*. We confirmed that the expression of these transgenes driven by *Act5C-GAL4* were comparable using immunoblotting against FLAG (Figures S1F and S1G).

To examine the localization of exogenously expressed dPTPMT1, we performed mitochondrial enrichments using adults or larvae with ubiquitous expression of each of our transgenes. We used the inner mitochondrial membrane protein, dMIC60, as a positive control for enrichment of mitochondria (Tsai et al., 2018). Exogenously expressed dPTPMT1-WT-3×FLAG was detected in the mitochondrial-enriched fraction, although it was also detected in the cytosolic fraction (Figure S1H). Deletion of the putative MTS decreased dPTPMT1-3×FLAG levels in the mitochondrial-enriched fraction (Figure S1I), suggesting that the N-terminal amino acids 1–31 direct dPTPMT1 import into mitochondria. These results are consistent

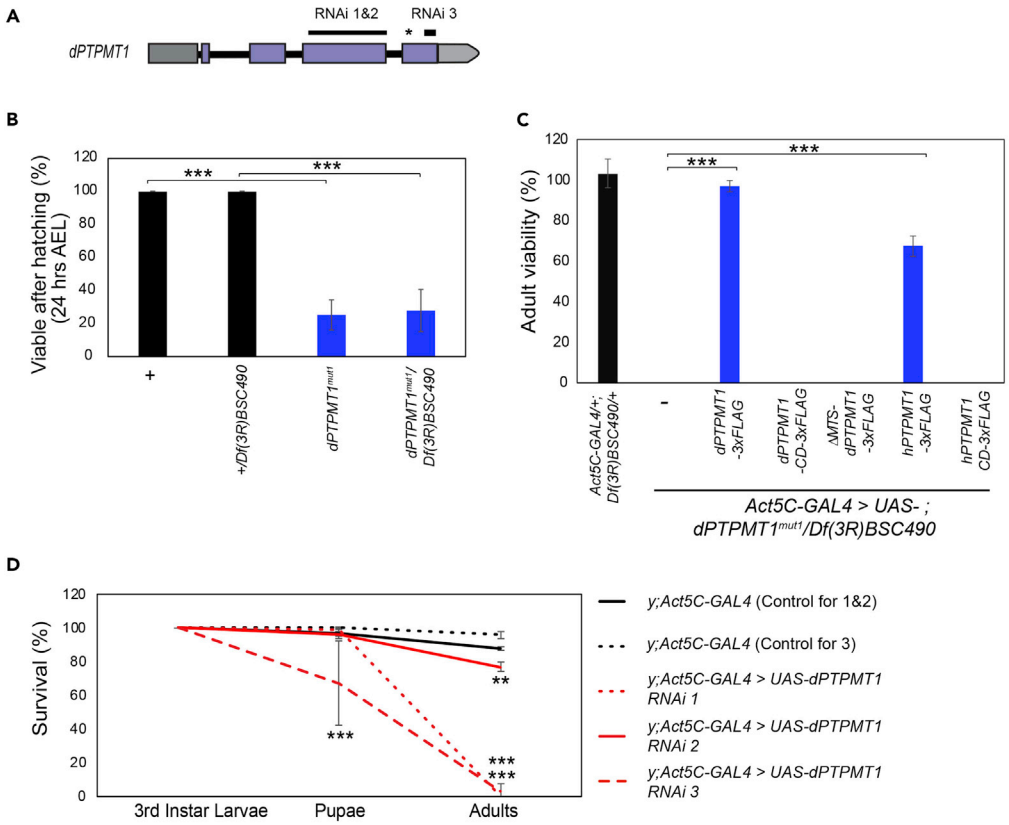

Figure 1. *dPTPMT1* Is an Essential Gene in *Drosophila*

(A) Regions in *dPTPMT1* targeted by the three RNAi lines. Thin black bars indicate regions targeted by RNAi, dark gray bar is the 5′ UTR, light gray bar is the 3′ UTR, purple bars are exons, and thick black bars are introns. Asterisk indicates the location of the deletion in $dPTPMT1^{mut1}$.

(B) Viability of $dPTPMT1^{mut1}$ first instar larvae at 24 h AEL. n = 4–5 replicates, 56–285 for each repeat. Data are represented as mean ± SEM and ***p < 0.001 by chi-square test.

(C) Adult viability of $dPTPMT1^{mut1}$ mutants. Genotypic frequency is calculated for adults and then normalized to expected genotypic frequency. n = 3–4 replicates; 0- to 2-day-old adults. Data are represented as mean ± SEM and ***p < 0.001 by chi-square test.

(D) Percentage of third instar males with ubiquitous *dPTPMT1* RNAi surviving to pupation and eclosion. Larvae are on a yellow mutant background (hereafter indicated by "*y*"). Statistical significance is given relative to *Act5C-GAL4* crossed to the respective RNAi background controls at the same developmental stage. n = 3 replicates, 25–26 for each repeat for RNAi 1-2 and controls. n = 3 replicates, 12–44 for each repeat for RNAi 3 and control.

Data are represented as mean ± SEM and **p < 0.01, ***p < 0.001 by chi-square test. See also Figure S1.

with a previous study in yeast showing that heterologously expressed dPTPMT1 localizes to mitochondria (Teh et al., 2013). Importantly, dPTPMT1-CD-3×FLAG was also detected in the mitochondrial fraction (Figure S1J). We next assayed flies with ubiquitous expression of *UAS-hPTPMT1-WT-3×FLAG* and *UAS-hPTPMT1-CD-3×FLAG* and detected both versions of hPTPMT1 in the mitochondrial fraction (Figure S1K). Collectively, the generation of these transgenes allowed us to perform the following functional studies of PTPMT1 in flies.

To corroborate that the lethality observed in *dPTPMT1* CRISPR mutants was caused by a lack of dPTPMT1, we ubiquitously expressed *UAS-dPTPMT1-3×FLAG* in $dPTPMT1^{mut1}$ transheterozygotes. Ubiquitous expression of *UAS-dPTPMT1-3×FLAG* allowed mutants to survive to adulthood, eclosing at the expected genotypic ratio (Figure 1C). This result confirms that the lethality of *dPTPMT1* CRISPR mutants is caused by the loss of dPTPMT1. It should be noted that we were unable to quantify viability in this rescue experiment by counting the numbers of survivors of larvae and pupae as implemented in Figure 1D, because one of the lines necessary for the identification of genotypes of third instars could not be generated. Instead, we quantified viability by calculating the genotypic ratio of surviving adults and then normalizing it to the

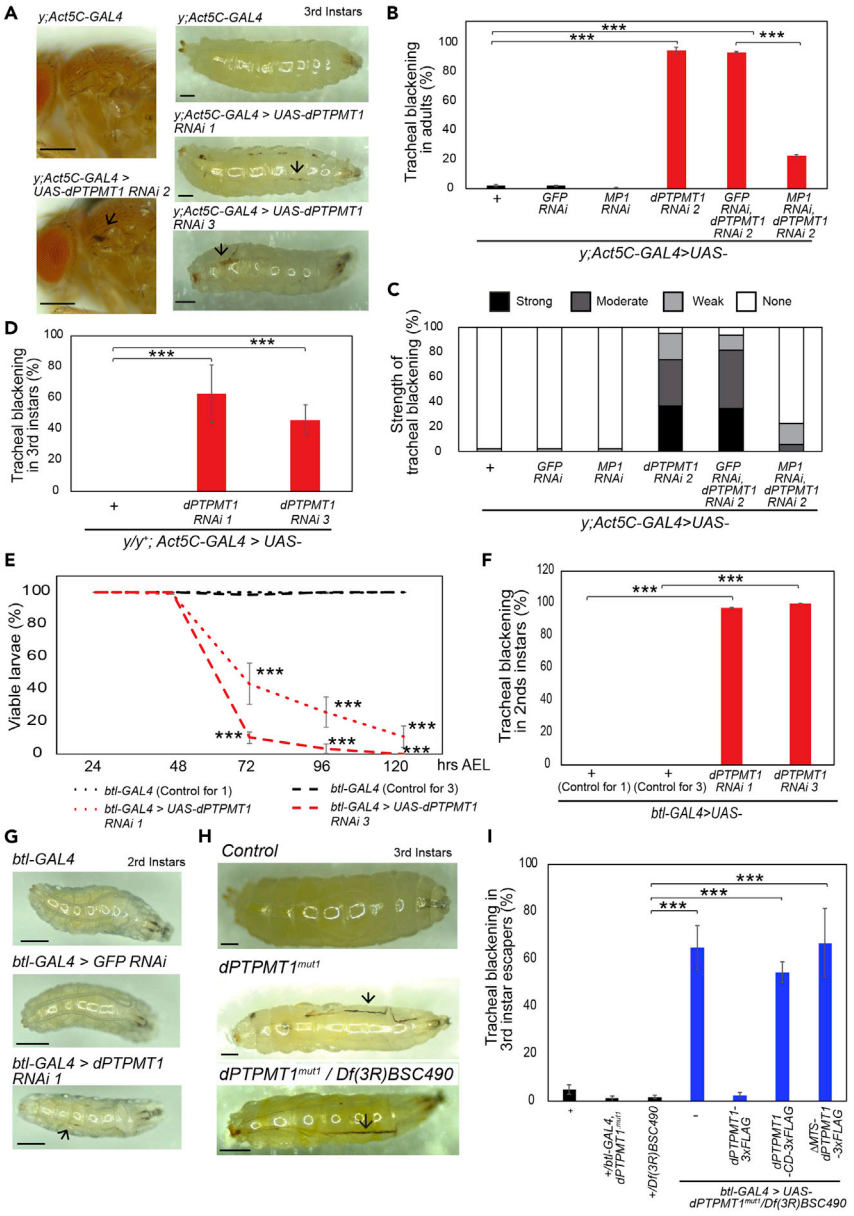

Figure 2. dPTPMT1 Depletion Results in Tracheal Blackening

(A) Ubiquitous *dPTPMT1* RNAi results in tracheal blackening (arrows); 0- to 2-day-old adult males and third instar males are shown. Scale bars, 250 μm.

(B and C) Percentage of 0- to 2-day-old adult males with tracheal blackening (B) and strength of tracheal blackening (C). n = 3 replicates, 48–138 for each repeat. Data are represented as mean ± SEM and ***p < 0.001 by chi-square test.

(D) Percentage of third instars with tracheal blackening; mixed-sex, females are heterozygous for *y* and males are hemizygous for *y* (hereafter denoted as y/y^{+}). n = 3 replicates, 25–43 for each repeat. Data are represented as mean ± SEM and ***p < 0.001 by chi-square test.

(E) Viability of tracheal-specific *dPTPMT1* RNAi larvae. Statistical significance is given relative to *btl-GAL4* crossed to respective RNAi background controls at the same developmental stage. n = 2–3 replicates, 50–100 for each repeat. Data are represented as mean ± SEM and ***p < 0.001 by chi-square test.

(F) Percentage of second instar, tracheal-specific *dPTPMT1* RNAi larvae with tracheal blackening. n = 2–3 replicates, 38–94 for each repeat. Data are represented as mean ± SEM and ***p < 0.001 by chi-square test.

Figure 2. *Continued*
(G) A representative image of a second instar larva with tracheal-specific *dPTPMT1* RNAi shows tracheal blackening (arrow). Scale bars, 250 μm.
(H) Tracheal blackening (arrows) in $dPTPMT1^{mut1}$ third instar larvae. Scale bars, 250 μm.
(I) Percentage of $dPTPMT1^{mut1}$ third instars with tracheal blackening. n = 2–4 replicates, 16–110 for each repeat.
Data are represented as mean ± SEM and ***p < 0.001 by chi-square test. See also Figures S2 and S3.

expected genotypic frequency. Importantly, expression of *ΔMTS-dPTPMT1-3×FLAG* and *dPTPMT1-CD-3×FLAG* failed to rescue viability of CRISPR mutants (Figure 1C), indicating that mitochondrial localization and catalytic activity are required for dPTPMT1's function. Ubiquitous expression of *UAS-hPTPMT1-WT-3×FLAG*, but not *UAS-hPTPMT1-CD-3×FLAG*, was also able to rescue viability (Figure 1C), indicating that human and fly PTPMT1 are functionally conserved. Notably, expression of *dPTPMT1* in specific tissues such as the trachea by *btl-GAL4*, neurons by *elav-GAL4*, or muscles by *Mhc-GAL4* did not rescue the viability of $dPTPMT1^{mut1}$ transheterozygotes, indicating that dPTPMT1 is required in multiple tissues in *Drosophila* for survival. Collectively, these data suggest that *dPTPMT1* is essential for viability in the fly.

Depletion of dPTPMT1 Causes Tracheal Blackening

We noticed that ubiquitous *dPTPMT1* RNAi resulted in tracheal blackening in both adults and third instar larvae (Figure 2A). All three *dPTPMT1* RNAi lines showed a significantly higher frequency of tracheal blackening than controls (Figures 2B–2D). By contrast, ubiquitous *GFP* RNAi did not cause significant tracheal blackening, indicating that this phenotype is not an artifact of the RNAi system (Figures 2B and 2C). Using transmission electron microscopy (TEM) on a section of trachea from a third instar larva with ubiquitous *dPTPMT1* RNAi, we discovered large electron-dense regions between the tracheal cuticle and the tracheal epithelial cells (Figure S2A). To test whether this tracheal blackening was due to melanization, we used RNAi to ubiquitously knockdown *MP1*, a serine protease reported to be involved in activating tracheal melanization (Tang et al., 2006, 2008). Using qPCR, we confirmed a significant reduction of *MP1* transcripts (Figure S2B). We saw a substantial decrease in the strength and frequency of tracheal blackening in *dPTPMT1* RNAi flies by *MP1* RNAi but not by *GFP* RNAi (Figures 2B and 2C). These results indicate that tracheal blackening is at least partially a result of melanization.

To determine whether this blackening phenotype was cell autonomous, we performed a tracheal-specific RNAi knockdown of *dPTPMT1*, using *btl-GAL4* (Kim et al., 2018). Both *dPTPMT1* RNAi 1 and 3 resulted in early lethality (Figure 2E). We found that over half of *dPTPMT1* RNAi larvae were dead by 72 h AEL (Figure 2E). It should be noted that, in this particular experiment at 72 h AEL, the majority of larvae (control and RNAi) were second instars (Figure S2C), due to the developmental delay caused by sorting first instars at room temperature (22°C) at hatching (see Methods). Many of these larvae were found dead on the side of the vial, suggesting that they died of anoxia as second instar larvae (Wagner et al., 2009). Importantly, first instar larvae with tracheal *dPTPMT1* RNAi showed no sign of tracheal blackening (*btl-GAL4*—Control for RNAi 1: 0% ± 0%, *btl-GAL4>UAS-dPTPMT1* RNAi 1: 0% ± 0%; *btl-GAL4*—Control for RNAi 3: 0% ± 0%, *btl-GAL4>UAS-dPTPMT1* RNAi 3: 1% ± 1%; n = 2–3 replicates, 37–97 for each repeat). However, nearly all second instar larvae had blackened trachea (Figures 2F and 2G). TEM on a section of trachea from a third instar escaper with tracheal-specific *dPTPMT1* RNAi also revealed large electron-dense regions between the tracheal cuticle and the tracheal epithelial cells (Figure S2D), like ubiquitous *dPTPMT1* RNAi (Figure S2A). Therefore, tracheal blackening occurs during the transition from first to second instar in tracheal-specific *dPTPMT1* RNAi larvae.

Melanization can be activated by the trachea (Tang et al., 2008). However, it can also be mediated by phenol oxidases, released by crystal cells, in the hemolymph (Tang, 2009). Knockdown of *MP1* specifically in the trachea has been shown to block tracheal-specific melanization (Tang et al., 2008). To determine whether tracheal blackening in *dPTPMT1 RNAi* larvae was a result of tracheal-specific melanization being activated, we knocked down *MP1* in the trachea by *btl-GAL4*. Tracheal-specific *MP1* RNAi did not reduce tracheal blackening; however, it did partially rescue viability (Figures S2E and S2F), suggesting that MP1 mediates tracheal blackening through other tissues in *dPTPMT1 RNAi*.

Data from Flybase (www.flybase.org) show that *dPTPMT1* is ubiquitously expressed. To determine whether dPTPMT1 is required in non-tracheal tissues to prevent tracheal blackening, we knocked down *dPTPMT1* using drivers specific to the nervous system (multiple *elav-GAL4* drivers and *ey-GAL4*), the muscles (*Mhc-GAL4* and *C57-GAL4*), and the fat bodies/hemocytes (*Pxn-GAL4*, *Cg-GAL4*). *dPTPMT1*

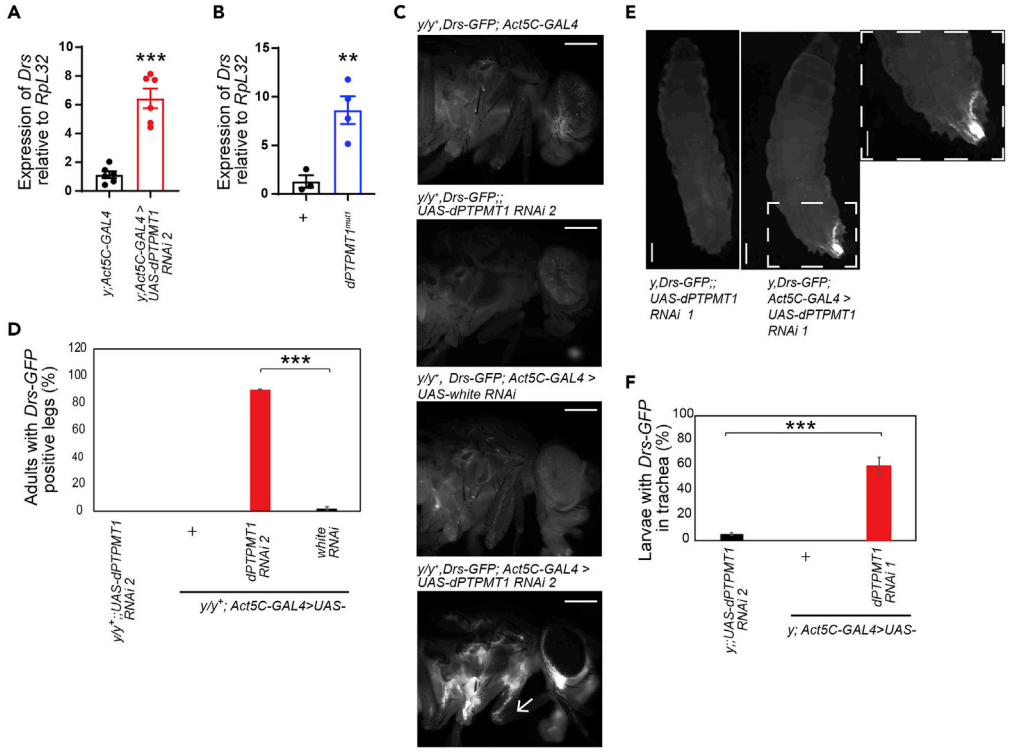

Figure 3. dPTPMT1 Depletion Results in *Drs* Expression in the Trachea

(A and B) (A) qPCR analysis of *Drs* expression using whole-fly lysates. n = 3–6 replicates of 15–20 0- to 2-day-old adult males (A) or third instars (B). Data are represented as mean ± SEM and **p < .01, ***p < 0.001, by one-tailed Student's t test.

(C) *Drs-GFP* expression in *dPTPMT1* RNAi adult females, 0–2 days old. Arrow points to signal in the leg trachea. Females are heterozygous for *y* mutation (y/y^+). Scale bars, 250 μm.

(D) Percentage of adult females with *Drs-GFP* in the trachea. Females are heterozygous for *y* mutation (y/y^+). n = 3 replicates, 17–57 for each repeat, 0–2 days old. Data are represented as mean ± SEM and ***p < 0.001 by chi-square test.

(E) *Drs-GFP* expression in *dPTPMT1* RNAi third instar males. Arrow points to *Drs-GFP* expression in the dorsal trunk of the trachea and posterior spiracles. Dashed box shows a higher magnification image of the affected area. Scale bars, 250 μm.

(F) Percentage of third instar males with *Drs-GFP* expression in the trachea. n = 4–7 replicates, 12–53 for each repeat. Data are represented as mean ± SEM and ***p < 0.001 by chi-square test. See also Figure S3.

RNAi by these drivers did not result in any apparent lethality, blackening phenotypes, or other visible phenotypes (Figure S2G), suggesting that tracheal epithelial cells are highly sensitive to loss of *dPTPMT1*.

Next, we examined *dPTPMT1* CRISPR mutants and found that third instar escapers from all three CRISPR lines showed substantial tracheal blackening as homozygotes and transheterozygotes (Figures 2H, 2I, S3A, and S3B). Ubiquitous expression of dPTPMT1 in $dPTPMT1^{mut1}$ transheterozygotes resulted in no tracheal blackening in rescued adults (n = 4 replicates, 47–58 adults for each repeat). Interestingly, although ubiquitous expression of *hPTPMT1-3×FLAG* rescued viability in $dPTPMT1^{mut1}$ transheterozygotes (Figure 1C), 20% of these adults showed tracheal blackening (n = 3 replicates, 29–48 adults for each repeat). Importantly, ubiquitous expression of *hPTPMT1* but not *hPTPMT1-CD* also caused tracheal blackening in a wild-type background. Twenty percent of adults with *hPTPMT1* expression showed tracheal blackening compared with 0% of adults with *hPTPMT1-CD* expression (n = 3 replicates, 10 adults for each repeat), suggesting that hPTPMT1 acts as a weak dominant negative for tracheal blackening in *Drosophila*. We were also able to rescue tracheal blackening in $dPTPMT1^{mut1}$ transheterozygotes with tracheal-specific expression of wild-type *dPTPMT1-3×FLAG* but not *CD* or *ΔMTS-dPTPMT1-3×FLAG* (Figure 2I). Collectively, these data demonstrate that dPTPMT1 is essential to prevent tracheal blackening in a cell-autonomous manner and this function is dependent upon dPTPMT1's mitochondrial localization and phosphatase activity.

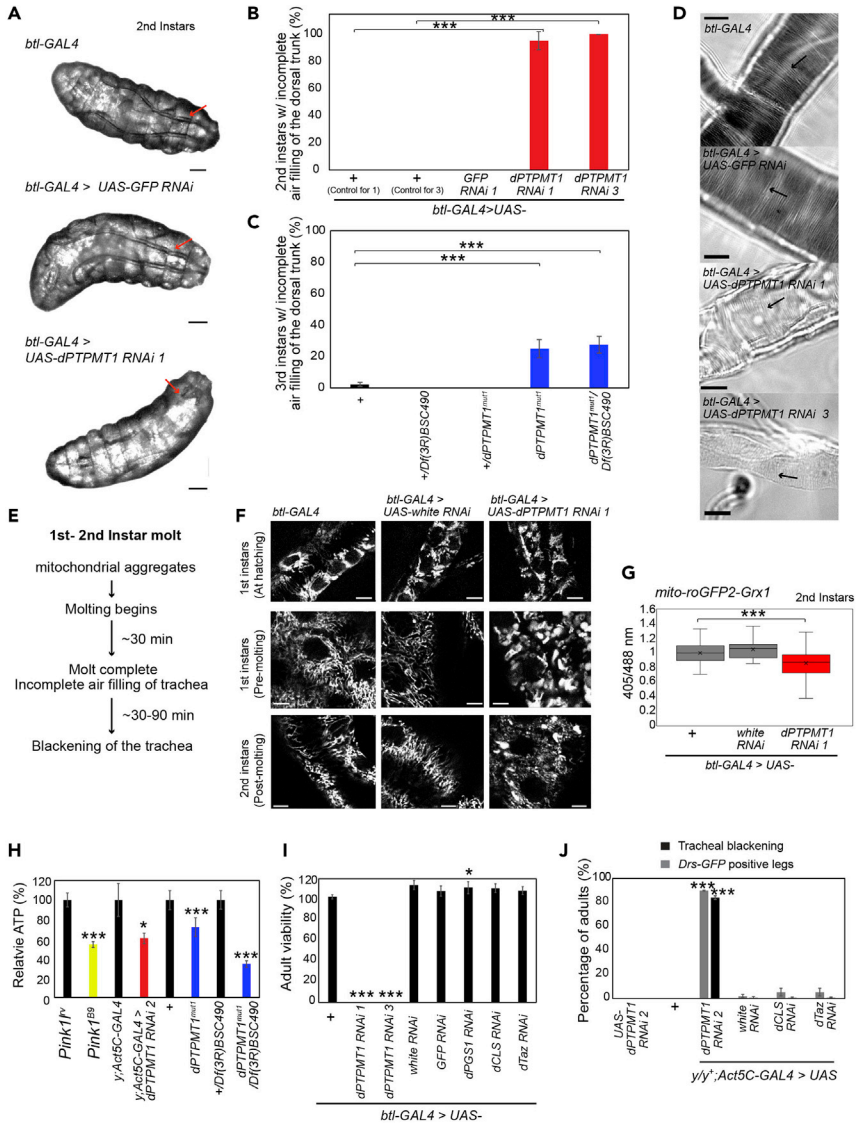

Figure 4. dPTPMT1 Depletion Results in Air Filling and Mitochondrial Defects in the Trachea

(A) Air-filling defects in second instars with tracheal-specific *dPTPMT1* RNAi. Red arrows indicate trachea. In *dPTPMT1* RNAi a portion of the posterior dorsal trunk shows air filling, but the remainder of the dorsal trunk is unfilled. Trachea filled with air appears darker than the adjacent tissues owing to differences in the refractive indices of liquid and air. Scale bars, 100 μm.

(B) Percentage of second instars with air-filling defects with tracheal-specific *dPTPMT1* RNAi. n = 3 replicates, 6–12 for each repeat. Data are represented as mean ± SEM and ***p < 0.001 by chi-square test.

(C) Percentage of $dPTPMT1^{mut1}$ third instars showing tracheal air-filling defects. n = 3–6 replicates, 14–33 for each repeat. Data are represented as mean ± SEM and ***p < 0.001 by chi-square test.

(D) Taenidial folds (arrows) in dissected trachea captured by light microscopy show no defects in tracheal-specific *dPTPMT1* RNAi second instars. Note that these mutant tracheae are transparent because of the lack of air. The same results were seen in 8–22 larvae from two independent crosses. Scale bars, 100 μm.

(E) Timeline of events in tracheal-specific *dPTPMT1* RNAi larvae undergoing first to second instar molt.

(F) Live imaging of mito-GFP within the dorsal trunk of the trachea of first instars at hatching, just prior to molting ("pre-molting"), and newly molted second instars ("post-molting"). The same results were seen in ten larvae from two independent crosses. Scale bars, 5 μm.

(G) Quantification of fluorescence ratios of mito-roGFP2-Grx1 expressed in trachea of second instars. n = 32–38 from three independent crosses. Boxes show 25th/75th percentiles, whiskers are the minimum and maximum values, and x is the median marker and ***p < 0.001 by one-tailed Student's t test.

Figure 4. *Continued*

(H) Relative ATP levels, normalized to total protein. n = 7 independent experiments. Five-day-old *Pink11*^{RV} (control) and *Pink1*^{B9} adult males (Park et al., 2006) were used as a positive control. Ubiquitous *dPTPMT1* RNAi were adult males (0–2 days old) and *dPTPMT1*^{mut1} were third instars. Statistical significance is given relative to respective controls (black bar). Data are represented as mean ± SEM and *p < 0.05, ***p < 0.001 by one-tailed Student's t test.

(I) Viability of adults with tracheal-specific RNAi of enzymes involved in CL biosynthesis raised at 25°C, 0- to 2-day-old adults. For simplicity only one background control is shown. Genotypic frequency is calculated for the genotype of interest and then normalized to its expected genotypic frequency. Statistical significance is given relative to respective controls. *dPGS1* RNAi viability is significantly increased relative to its control. Data are represented as mean ± SEM and *p < 0.05, ***p < 0.001 by chi-square test.

(J) Tracheal blackening and *Drs-GFP* expression in adult females (0–2 days old) with ubiquitous RNAi of CL biosynthesis enzymes. Females are heterozygous for *y* mutation (*y*/*y*$^{+}$). Statistical significance is given relative to *Act5C-GAL4>white* RNAi. n = 3 replicates, 17–83 for each repeat. Data for *Drs-GFP* for controls and *dPTPMT1* RNAi are the same as in Figure 3D.

Data are represented as mean ± SEM and ***p < 0.001 by chi-square test. See also Figures S3 and S4.

dPTPMT1 Depletion Results in *Drosomycin* Expression in the Trachea

Because tracheal melanization has been shown to induce the expression of one of the AMPs, *Drosomycin (Drs)* (Tang et al., 2008), we assayed *dPTPMT1* RNAi and CRISPR mutant larvae for expression of *Drs*. qPCR revealed that *Drs* was significantly upregulated in ubiquitous *dPTPMT1* RNAi adults and in *dPTPMT1*^{mut1} homozygous third instar escapers (Figures 3A and 3B). Ubiquitous *dPTPMT1* RNAi third instars also showed increased *Drs* expression by qPCR, although this increase was not statistically significant (Figure S3C). We next examined localization of *Drs-GFP* expression in adults and third instar larvae with ubiquitous *dPTPMT1* RNAi, using *Drs-GFP* reporter flies (Ferrandon et al., 1998). We saw an increased percentage of both adults and larvae with *Drs-GFP* expression in their trachea (Figures 3C–3F). We also examined *Drs-GFP* in *white* RNAi trachea, which have a knockdown of the transporter involved in pigmentation of the eye (Mount, 1987). We did not see a significant increase in the percentage of *white* RNAi adults with *Drs-GFP* in the trachea (Figures 3C and 3D), indicating that the lack of dPTPMT1, rather than the RNAi system itself, is responsible for this phenotype.

Lastly, we asked whether tracheal blackening and *Drs* elevation were specific to the loss of *dPTPMT1*, or a general by-product of mitochondrial dysfunction. To answer this question, we examined larvae lacking *dMIC60*, a key mitochondrial player for maintaining mitochondrial structure and function (Tsai et al., 2017, 2018). We found that only 2.3% of third instars (n = 86) had tracheal blackening as compared with 46%–100% in *dPTPMT1* mutants and only 7% had tracheal *Drs-GFP* expression (±4% versus *w*^{1118} control: 0% ± 0%, n = 2–3 replicates, 10–28 for each repeat) as compared with 59%–90% in *dPTPMT1* mutants. This result suggests that tracheal blackening and *Drs* elevation are unlikely non-specific responses to general mitochondrial dysfunction. Taken together, dPTPMT1 is required to prevent both tracheal blackening and *Drs* upregulation.

dPTPMT1 Depletion Causes Tracheal Air-Filling Defects

Because we found that tracheal blackening was absent in first instar larvae with tracheal-specific *dPTPMT1* RNAi, but highly penetrant in second instars, we performed an in-depth examination of these larvae during the first-second instar molt. We inspected the trachea of *dPTPMT1* RNAi first instars and discovered that these mutants failed to fill their trachea with air upon completion of molting (Figures 4A and 4B). Failure of tracheal air filling was only observed in *dPTPMT1* RNAi but not in *GFP* RNAi larvae (Figures 4A and 4B). First instars with tracheal-specific *dPTPMT1* RNAi examined at hatching (24 h AEL, n = 5, *btl-GAL4 > UAS-dPTPMT1* RNAi 1, *UAS-mito-GFP*) and just prior to molting (48 h AEL, n = 5, *btl-GAL4 > UAS-dPTPMT1* RNAi 1, *UAS-mito-GFP*) showed no air-filling defects in the trachea, suggesting that these defects occur during or immediately following molting. We examined *dPTPMT1*^{mut1} homozygous and transheterozygous third instar escapers and found that they also showed defects in tracheal air filling, although this phenotype was less penetrant, possibly due to genetic backgrounds and the resistance of escapers to stressors (Figure 4C). In addition, TEM on the trachea of a third instar larva with ubiquitous *dPTPMT1* RNAi and on a larva with tracheal-specific *dPTPMT1* RNAi revealed that the tracheal lumina of these larvae were filled with unidentifiable membranous materials as well as what we presumed to be molting fluid (Figures S2A and S2D). Together, these data show that *dPTPMT1* mutants fail to fill their trachea with air and fail to clear fluid from the tracheal lumen.

To exclude the possibility that structural defects were responsible for failed fluid clearance and air filling, we examined the taenidia of second instars and saw no obvious defects in the structure of taenidia in either

of our two independent RNAi lines, despite the obvious lack of air in their trachea (Figure 4D). TEM on third instar larvae with ubiquitous and tracheal-specific *dPTPMT1* RNAi did show some abnormally formed taenidia (Figures S2A and S2D). This result suggests that these tracheal phenotypes are not caused by gross cuticular defects; however, subtler defects in taenidial structure may play a role.

To determine the temporal relationship between failure of air filling and tracheal blackening, we performed a time course analysis. We found that failure of air filling was followed by blackening of the trachea, within 30–90 min of molting completion (n = 15–17, 2 independent crosses) (Figure 4E). Importantly, although we observed nearly complete penetrance of both tracheal blackening and tracheal air filling defects in tracheal-specific *dPTPMT1* RNAi larvae (Figures 2F and 4B), we found that $dPTPMT1^{mut1}$ homozygous and transheterozygous third instar escapers showed a higher frequency of tracheal blackening than air-filling defects (Figures 2I and 4C). These results suggest that, although the failure of tracheal air filling precedes tracheal blackening in tracheal-specific *dPTPMT1* RNAi, the air-filling failure is not absolutely required for blackening. It is likely both phenotypes are a consequence of an initial defect in the trachea due to a lack of dPTPMT1.

dPTPMT1 Depletion Leads to Mitochondrial Aggregates Prior to Failure of Air Filling

We set out to search for any defect that occurred earlier than tracheal air-filling failure and blackening in our mutants. Because dPTPMT1 is a mitochondrially localized phosphatase, we hypothesized that *dPTPMT1* deficiency disrupted mitochondrial function in tracheal epithelial cells, which consequently interfered with air filling during molting. We examined mitochondrial function in first and second instars with tracheal-specific *dPTPMT1* RNAi by *btl-GAL4*, because they showed a strong, penetrant phenotype with a precise onset.

We expressed *UAS-mito-GFP* in tracheal-specific *dPTPMT1* RNAi larvae and live-imaged mito-GFP within the trachea. We found that, although mito-GFP signal appeared normal at hatching, enlarged mito-GFP puncta started to form just prior to molting in first instars and persisted in recently molted second instars (Figure 4F). At both developmental stages, these puncta were present throughout the dorsal trunk and tracheal branches. Notably, there was a greater number of large mito-GFP puncta in late first instars than in early second instars (Figure 4F). Importantly, this mitochondrial phenotype preceded the air-filling phenotype (Figure 4E). To exclude the possibility that these mito-GFP puncta were an artifact of our RNAi system, we examined mito-GFP in the trachea of larvae with tracheal-specific knockdown of *white*. In these larvae, mito-GFP appeared normal, as in controls (Figure 4F). Large mito-GFP puncta were also present in *dPTPMT1* RNAi trachea using two additional independent mitochondrially localizing GFP lines (Figure S3D). These large, irregular mito-GFP puncta may represent clusters of mitochondria. Indeed, under TEM we saw individual mitochondria with intact crista structure aggregated in a tracheal epithelial cell of a third instar escaper with tracheal-specific *dPTPMT1* RNAi (Figure S3E). To eliminate the possibility that the air-filling failure we observed in *dPTPMT1* mutants was a result of tracheal epithelial cell death, we examined tracheal cells using terminal deoxynucleotidyl transferase dUTP nick end labeling (TUNEL) staining. We saw no significant differences in the number of TUNEL-positive cells between mutants and controls (Figure S3F), suggesting that *dPTPMT1*-depleted tracheal epithelial cells are not apoptotic. Collectively, these results suggest that a defect in mitochondria could be the earliest phenotype in *dPTPMT1* mutant trachea (Figure 4E).

dPTPMT1 Depletion Compromises Mitochondrial ROS Production in the Trachea and ATP Levels

Defective tracheal air filling causes anoxia, which consequently impacts mitochondrial aerobic respiration. We examined mitochondrial reactive oxidative species (ROS), which are a key by-product of mitochondrial oxidative phosphorylation, in tracheal epithelial cells. We used two genetically encoded mitochondrial ROS sensors: *UAS-mito-roGFP2-Grx1*, a reporter of the glutathione redox potential, which indicates general ROS and reactive nitrogenous species (RNS) (Lushchak, 2012), and *UAS-mito-roGFP2-Orp1*, a hydrogen peroxide (H_2O_2) sensor (Albrecht et al., 2011; Barata and Dick, 2013). roGFPs are redox-sensitive GFPs that react to oxidants and reductants, resulting in ratiometric changes in fluorescence emitted at 500–530 nm when the probe is excited at 405 and 488 nm (Dooley et al., 2004; Hanson et al., 2004). An increase in the 405/488 nm ratio indicates increased oxidant concentration. Coupling roGFP to Grx1 and Orp1 enhances its specificity for glutathione and H_2O_2, respectively (Gutscher et al., 2008, 2009). We did not observe significant differences in the fluorescence ratio (405/488 nm) of the two ROS reporters between controls and tracheal-specific RNAi of *dPTPMT1* by *btl-GAL4* at 24 h AEL (first instars) (Figures S3G and

S3H). However, we did see a significant decrease in the fluorescence ratio of *mito-roGFP2-Grx1* in second instars of *dPTPMT1* RNAi (Figure 4G). We also detected a decrease in H_2O_2 levels as measured by *mito-roGFP2-Orp1* in second instars of *dPTPMT1* RNAi, although this difference was not statistically significant (Figure S3H). These results indicate reduced ROS levels in *dPTPMT1* RNAi. The timing of the occurrence of ROS reduction coincided with the failure of tracheal air filling in *dPTPMT1* RNAi. Both phenotypes were not present in first instars but were present after molting in second instars. It is likely that the lack of air within the trachea reduced mitochondrial oxidative phosphorylation and consequently decreased ROS generation. Consistent with this hypothesis, ubiquitous *dPTPMT1* RNAi adults, $dPTPMT1^{mut1}$ homozygous, and transheterozygous third instar escapers all showed lowered ATP levels (Figure 4H). We used $Pink1^{B9}$ adult males, which have been reported to show decreased ATP levels, to validate our ATP assay (Park et al., 2006). Taken together, our findings demonstrate that the lack of dPTPMT1 compromises mitochondrial ROS production in the trachea and reduces ATP levels.

Depletion of the CL Pathway Components Does Not Mimic *dPTPMT1* Deficiency

Next, we set out to explore the underlying molecular mechanism by which *dPTPMT1* deficiency causes tracheal air-filling failure and immune activation. Because we have demonstrated that the catalytic activity of dPTPMT1 is required to prevent tracheal blackening in *dPTPMT1* mutants, we reasoned that dPTPMT1 might act through its known substrates. PTPMT1 has been implicated in CL synthesis in mammals (Figure S4A), acting as a phosphatidylglycerophosphate (PGP) phosphatase (Zhang et al., 2011). It has been found that dPTPMT1 dephosphorylates PGP to phosphatidylglycerol (PG) *in vitro* (Teh et al., 2013). Furthermore, expression of *dPTPMT1* in yeast deficient for the PGP phosphatase, GEP4, rescues decreased viability (Teh et al., 2013), suggesting that PTPMT1's role as a PGP phosphatase may be conserved in the fly.

To determine whether loss of dPTPMT1 causes tracheal phenotypes via the CL pathway, we examined tracheal phenotypes in mutants lacking additional enzymes involved in CL synthesis. We identified a *Drosophila* homolog (CG7718: dPGS1) of mammalian phosphatidylglycerophosphate synthase 1 (PGS1), which acts upstream of PTPMT1 in CL synthesis (Figure S4A) (Kawasaki et al., 1999). dPGS1 shares 43% identity to the amino acid sequence of human PGS1. We also tested CL synthase (CG4774; dCLS) and tafazzin (CG8766; dTaz), which act downstream of PTPMT1 in CL synthesis (Figure S4A) (Xu et al., 2006; Acehan et al., 2011; Dudek, 2017). Using qPCR, we confirmed significant knockdown of *dPGS1*, *dCLS*, and *dTaz* by RNAi (Figure S4B). None of these RNAi lines were lethal when driven by the tracheal-specific driver, *btl-GAL4*, at 25°C or 30°C (Figures 4I and S4C). Furthermore, none of the surviving adults showed tracheal blackening. We also examined adults with ubiquitous RNAi of *dCLS* and *dTaz* driven by *Act5C-GAL4* and did not see tracheal blackening or expression of *Drs-GFP* in the trachea (Figures 4J and S4D). Ubiquitous *dPGS1* RNAi was pupal lethal, so we examined third instars and again saw no expression of *Drs-GFP* in the trachea, no tracheal blackening, and no tracheal air-filling defects (n = 51–56 third instar female larvae). We further examined third instars of *dCLS* mutants ($dCLS^{e01021}$/$dCLS^{C01874}$) (Thibault et al., 2004) and saw no evidence of tracheal blackening (w^{1118} control: 1% ± 0% versus *dCLS* mutant 0% ± 0%; n = 2–3 replicates, 22–102 third instar larvae for each repeat), consistent with our findings with *dCLS* RNAi. Together, these data suggest that the CL biosynthesis pathway is not responsible for the defects observed in the tracheal system with dPTPMT1 deficiency.

DISCUSSION

In this paper, we have revealed a physiological role of dPTPMT1 in the *Drosophila* tracheal system. Loss of dPTPMT1 causes a sequence of defects in the trachea. In first instar larvae, with tracheal-specific *dPTPMT1* RNAi, we have observed mitochondrial clustering just prior to molting. These defects are followed by a failure to fill the trachea with air upon completion of molting and subsequent blackening of the trachea. We have provided evidence suggesting the hypoxic impacts of tracheal air-filling defects on mitochondria, including compromised mitochondrial ROS production and decreased ATP levels. Immune responses are also activated in these mutants, as demonstrated by MP1-dependent melanization and *Drs* upregulation. Our results show that the lack of dPTPMT1 in tracheal epithelial cells interferes with the ability of epithelial cells to perform air filling and activates immune responses.

To date, the mechanisms of tracheal air filling are poorly defined. Our current understanding suggests that this process involves the removal of liquid from the lumen through active and passive ion transport across epithelial cell membranes and the production of gas in the lumen through the dehydration of bicarbonate ions (Förster and Woods, 2013). Mitochondria play a key role in maintaining homeostasis of ions and metabolites and generating ATP to power ion exchanges. Mitochondrial metabolism and oxidative phosphorylation require a series of

biochemical reactions within the mitochondria. One possibility is that dPTPMT1 depletion causes a defect in a specific biochemical reaction in mitochondria, which subsequently impedes the ability of tracheal epithelial cells to conduct air filling. Interestingly, ablation of the carnitine acylcarnitine translocase, COLT, results in failure of air filling at the time of hatching, likely due to an energy deficiency from impaired fatty-acid oxidation (Oey et al., 2005; Hartenstein et al., 1997). It has been shown that loss of PTPMT1 in mammalian cell models causes decreased mitochondrial respiration, which in some cell types is accompanied by decreased ATP levels (Shen et al., 2011; Zhang et al., 2011; Yu et al., 2013; Zheng et al., 2018). In our fly models, we have observed reduced mitochondrial ROS production and decreased ATP levels (Figures 4G and 4H). The impairments in second instars appear to be a consequence of failed tracheal air filling; however, the lack of dPTPMT1 may also affect specific metabolic reactions that cause the mitochondrial aggregation observed in first instars prior to molting. It should be noted that general mitochondrial impairments are unlikely to be responsible for the sensitivity of tracheal epithelial cells to the loss of *dPTPMT1*, as we have not seen substantial tracheal blackening and *Drs-GFP* expression in *dMIC60* mutants (Tsai et al., 2017, 2018).

Although we speculate that the fluid detected within the lumen of affected tracheal cells is molting fluid, it is also possible that it is hemolymph that has infiltrated into the trachea as a result of disruptions in the integrity of the tracheal epithelium. Abnormal tracheal cell-cell junctions trigger tracheal air-filling failure owing to loss of the tracheal paracellular barrier (Ile et al., 2012). Additionally, deformations in the tracheal cuticle and taenidia have been connected with defects in tracheal air filling (Skouloudaki et al., 2019; Scholl et al., 2019; Jaspers et al., 2014; Yue et al., 2019; Rosa et al., 2018; Swanson et al., 2009). Light microscopy reveals no gross morphological defects in the taenidia of dPTPMT1-depleted trachea (Figure 4D), whereas TEM images show some abnormally formed taenidia (Figures S2A and S2D). However, it is difficult to assess the nature of these abnormalities owing to obliquities in sectioning, and this remains a possible explanation for air-filling failure in dPTPMT1 depletion.

Intriguingly, in mammals, one of PTPMT1's enzymatic products, PG, is the second most abundant phospholipid within lung surfactant—a mixture of lipids and proteins that reduces surface tension in the lung and prevents alveolar collapse (Agassandian and Mallampalli, 2013). PG is produced in the mitochondria and endoplasmic reticulum (Schlame et al., 1986; Agassandian and Mallampalli, 2013) and has critical functions in immunity in the lung surfactant (Kuronuma et al., 2009; Numata et al., 2010, 2012; Kandasamy et al., 2011). PTPMT1 may act in these organelles to generate PG for surfactant (Teh et al., 2013). Although there is currently no direct evidence that flies produce surfactant in the tracheal lumen (Förster and Woods, 2013), impairments in surfactant production could explain both the air-filling defects and immune activation demonstrated in *dPTPMT1* mutants. However, in our study, RNAi knockdown of *dPGS1*, which acts upstream of dPTPMT1 in the synthesis of PG, does not phenocopy *dPTPMT1* RNAi, suggesting that reduction of PG synthesis is not the reason for the activation of immune responses in mutant flies.

In addition to air-filling defects, we have observed blackening of the trachea following *dPTPMT1* RNAi. Tracheal blackening in ubiquitous *dPTPMT1* RNAi adults is partially blocked by knockdown of *MP1*, a known activator of PPO, which catalyzes melanization (Tang et al., 2006, 2008). Interestingly, tracheal-specific knockdown of *MP1* does not block tracheal blackening in *dPTPMT1* RNAi larvae, suggesting that melanization of the trachea is not cell autonomous but instead likely the result of melanization being activated by the hemolymph. Alternatively, this result could indicate that MP1 plays a dispensable role in the activation of tracheal-specific melanization, consistent with recent reports of its more redundant role in systemic immunity (Dudzic et al., 2019).

Notably, tracheal blackening occurs after the failure of gas filling in tracheal-specific *dPTPMT1* RNAi second instars. Tracheal blackening following failure of tracheal air filling has been reported elsewhere, although the mechanistic basis for this effect has not be elucidated (Fisk and Thummel, 1998; Xu et al., 2019). Although in our study tracheal epithelial cells show no evidence of apoptosis (Figure S3F), the possibility remains that these cells are undergoing necrosis, either prior to the occurrence of air-filling defects or following these defects as a result of hypoxia. Importantly, necrotic cells have been shown to activate innate immune pathways, including melanization and AMP expression, likely through damage-associated molecular patterns (DAMPs) (Chew et al., 2004; Link et al., 2007; Obata et al., 2014; Shaukat et al., 2015). Hypoxia may also directly activate immune responses (Abdelsadik, 2012; Bandarra et al., 2014). Flies grown in hypoxic conditions have been reported to activate AMP expression in the trachea, including *Drs* (Abdelsadik, 2012). Additionally, mitochondrial stress has been shown to lead to the release of mitochondrial DAMPs and the activation of innate immune responses (Nakahira et al., 2011; Zhou et al., 2011; Rongvaux

et al., 2014; White et al., 2014; West et al., 2015). These are a few explanations for the melanization and *Drs* elevation observed in the trachea, although our current study does not rule out a role for pathogens in the induction of these immune responses.

Our work using a *Drosophila* model of dPTPMT1 depletion adds to our understanding of the importance of dPTPMT1 in sustaining cellular and organismal functions. Mitochondrial activities mediated by dPTPMT1 likely determine the ability of tracheal epithelial cells to support air filling, which in turn enables mitochondrial oxidative phosphorylation and all essential cellular activities. Our *dPTPMT1* mutants and transgenes generated here will provide a useful toolkit to dissect the tissue-specific functions of dPTPMT1 and may help us elucidate additional roles for this phosphatase in mitochondrial biology.

Limitations of the Study

As mentioned in the text, tracheal sectioning for TEM was performed transversely, and thus obliquity in the sections limits our ability to make conclusions about defects in the taenidial ultrastructure. Although we described a number of tracheal phenotypes resulting from dPTPMT1 deficiency, the molecular mechanisms responsible for their manifestations remain undefined.

Resource Availability

Lead Contact

Further information and requests for resources and reagents should be directed to and will be fulfilled by the Lead Contact Xinnan Wang at xinnanw@stanford.edu.

Materials Availability

All unique/stable reagents generated in this study are available from the Lead Contact with a completed Materials Transfer Agreement.

Data and Code Availability

This study did not generate/analyze datasets/code.

METHODS

All methods can be found in the accompanying Transparent Methods supplemental file.

SUPPLEMENTAL INFORMATION

Supplemental Information can be found online at https://doi.org/10.1016/j.isci.2020.101285.

ACKNOWLEDGMENTS

This work was supported by the Department of Defense (PR150380, X.W.), Stanford Gabilan and McCormick Fellowship (X.W.), the Shurl and Kay Curci Foundation (X.W.), the Graduate Research Fellowship Program of the National Science Foundation (A.M.P.), and in part National Center for Research Resources (NCRR) (ARRA, 1S10RR026780-01). The contents of this work do not necessarily represent the official views of the NCRR or the National Institutes of Health. We thank Drs. Bingwei Lu, Liqun Luo, and Clarissa Cheney for providing flies; Drs. Melissa Harrison, Kate O'Connor-Giles, and Jill Wildonger for providing CRISPR plasmids; and Dr. John Perrino and the Stanford Cell Science Imaging EM Facility for support with TEM. We also thank Drs. Margaret Fuller, Richard Reimer, William Talbot, Vafa Bayat, Karen Mruk, Atossa Shaltouki, Pei-I Tsai, Chung-Han Hsieh, Roeland Vanhauwaert, Vinita Bharat, Li Li, Arnaldo Carreira-Rosario, Oguz Kanca, Catherine Baker, Jesse Isaacman-Beck, James Purzner, Susanna Brantley, and Cameron Berry, as well as Todd Galitz, Benjamin Bolival, Xue Yang, Teni Anbarchian, Julia Wucherpfennig, and Ashley Gonzalez for their advice and support.

AUTHOR CONTRIBUTIONS

A.M.P. designed and performed the experiments, analyzed the results, and wrote the manuscript. M.J.K. assisted with the CRISPR screen. X.W. supervised the project, designed the experiments, and wrote the manuscript.

DECLARATION OF INTERESTS

The authors declare no competing interests.

Received: April 5, 2020
Revised: May 28, 2020
Accepted: June 14, 2020
Published: July 24, 2020

REFERENCES

Abdelsadik, A.M.K. (2012). Hypoxia Induces Processes Related to Inflammation and Remodelling in the Airways of the Fruit Fly *Drosophila melanogaster* (Christian-Albrechts Universität Kiel).

Acehan, D., Malhotra, A., Xu, Y., Ren, M., Stokes, D.L., and Schlame, M. (2011). Cardiolipin affects the supramolecular organization of ATP synthase in mitochondria. Biophys. J. *100*, 2184–2192.

Agassandian, M., and Mallampalli, R.K. (2013). Surfactant phospholipid metabolism. Biochim. Biophys. Acta *1831*, 612–625.

Albrecht, S.C., Barata, A.G., Großhans, J., Teleman, A.A., and Dick, T.P. (2011). In vivo mapping of hydrogen peroxide and oxidized glutathione reveals chemical and regional specificity of redox homeostasis. Cell Metab. *14*, 819–829.

Bandarra, D., Biddlestone, J., Mudie, S., Muller, H.A., and Rocha, S. (2014). Hypoxia activates IKK–NF-κB and the immune response in *Drosophila melanogaster*. Biosci. Rep. *34*, e00127.

Barata, A.G., and Dick, T.P. (2013). In vivo imaging of H2O2 production in Drosophila. Methods Enzymol. *526*, 61–82, Elsevier.

Bergman, P., Esfahani, S.S., and Engström, Y. (2017). Drosophila as a model for human diseases—focus on innate immunity in barrier epithelia. Curr. Top. Dev. Biol. *121*, 29–81, Elsevier.

Chew, S.K., Akdemir, F., Chen, P., Lu, W.-J., Mills, K., Daish, T., Kumar, S., Rodriguez, A., and Abrams, J.M. (2004). The apical caspase dronc governs programmed and unprogrammed cell death in Drosophila. Dev. Cell *7*, 897–907.

Dietzl, G., Chen, D., Schnorrer, F., Su, K.-C., Barinova, Y., Fellner, M., Gasser, B., Kinsey, K., Oppel, S., and Scheiblauer, S. (2007). A genome-wide transgenic RNAi library for conditional gene inactivation in Drosophila. Nature *448*, 151–156.

Dooley, C.T., Dore, T.M., Hanson, G.T., Jackson, W.C., Remington, S.J., and Tsien, R.Y. (2004). Imaging dynamic redox changes in mammalian cells with green fluorescent protein indicators. J. Biol. Chem. *279*, 22284–22293.

Dudek, J. (2017). Role of cardiolipin in mitochondrial signaling pathways. Front. Cell Dev. Biol. *5*, 90.

Dudzic, J.P., Hanson, M.A., Iatsenko, I., Kondo, S., and Lemaitre, B. (2019). More than black or white: melanization and Toll share regulatory serine proteases in Drosophila. Cell Rep. *27*, 1050–1061.e3.

Ferrandon, D., Jung, A., Criqui, M.C., Lemaitre, B., Uttenweiler-Joseph, S., Michaut, L., Reichhart, J.M., and Hoffmann, J. (1998). A drosomycin–GFP reporter transgene reveals a local immune response in Drosophila that is not dependent on the Toll pathway. EMBO J. *17*, 1217–1227.

Fisk, G.J., and Thummel, C.S. (1998). The DHR78 nuclear receptor is required for ecdysteroid signaling during the onset of Drosophila metamorphosis. Cell *93*, 543–555.

Förster, T.D., and Woods, H.A. (2013). Mechanisms of tracheal filling in insects. Biol. Rev. *88*, 1–14.

Gratz, S.J., Cummings, A.M., Nguyen, J.N., Hamm, D.C., Donohue, L.K., Harrison, M.M., Wildonger, J., and O'Connor-Giles, K.M. (2013). Genome engineering of Drosophila with the CRISPR RNA-guided Cas9 nuclease. Genetics *194*, 1029–1035.

Gratz, S.J., Rubinstein, C.D., Harrison, M.M., Wildonger, J., and O'Connor-Giles, K.M. (2015). CRISPR-Cas9 genome editing in Drosophila. Curr. Protoc. Mol. Biol. *111*, 31.32.1–31.2.20.

Gutscher, M., Pauleau, A.-L., Marty, L., Brach, T., Wabnitz, G.H., Samstag, Y., Meyer, A.J., and Dick, T.P. (2008). Real-time imaging of the intracellular glutathione redox potential. Nat. Methods *5*, 553.

Gutscher, M., Sobotta, M.C., Wabnitz, G.H., Ballikaya, S., Meyer, A.J., Samstag, Y., and Dick, T.P. (2009). Proximity-based protein thiol oxidation by H2O2-scavenging peroxidases. J. Biol. Chem. *284*, 31532–31540.

Hanson, G.T., Aggeler, R., Oglesbee, D., Cannon, M., Capaldi, R.A., Tsien, R.Y., and Remington, S.J. (2004). Investigating mitochondrial redox potential with redox-sensitive green fluorescent protein indicators. J. Biol. Chem. *279*, 13044–13053.

Hartenstein, K., Sinha, P., Mishra, A., Schenkel, H., Török, I., and Mechler, B.M. (1997). The congested-like tracheae gene of *Drosophila melanogaster* encodes a member of the mitochondrial carrier family required for gas-filling of the tracheal system and expansion of the wings after eclosion. Genetics *147*, 1755–1768.

Ile, K.E., Tripathy, R., Goldfinger, V., and Renault, A.D. (2012). Wunen, a Drosophila lipid phosphate phosphatase, is required for septate junction-mediated barrier function. Development *139*, 2535–2546.

Jaspers, M.H., Pflanz, R., Riedel, D., Kawelke, S., Feussner, I., and Schuh, R. (2014). The fatty acyl-CoA reductase Waterproof mediates airway clearance in Drosophila. Dev. Biol. *385*, 23–31.

Kandasamy, P., Zarini, S., Chan, E.D., Leslie, C.C., Murphy, R.C., and Voelker, D.R. (2011). Pulmonary surfactant phosphatidylglycerol inhibits *Mycoplasma pneumoniae*-stimulated eicosanoid production from human and mouse macrophages. J. Biol. Chem. *286*, 7841–7853.

Kawasaki, K., Kuge, O., Chang, S.C., Heacock, P.N., Rho, M., Suzuki, K., Nishijima, M., and Dowhan, W. (1999). Isolation of a chinese hamster ovary (CHO) cDNA encoding phosphatidylglycerophosphate (PGP) synthase, expression of which corrects the mitochondrial abnormalities of a PGP synthase-defective mutant of CHO-K1 cells. The Journal of biological chemistry *274*, 1828–1834.

Kim, D.-H., Kim, Y.-J., and Adams, M.E. (2018). Endocrine regulation of airway clearance in Drosophila. Proc. Natl. Acad. Sci. U S A *115*, 1535–1540.

Kuronuma, K., Mitsuzawa, H., Takeda, K., Nishitani, C., Chan, E.D., Kuroki, Y., Nakamura, M., and Voelker, D.R. (2009). Anionic pulmonary surfactant phospholipids inhibit inflammatory responses from alveolar macrophages and U937 cells by binding the lipopolysaccharide-interacting proteins CD14 and MD-2. J. Biol. Chem. *284*, 25488–25500.

Link, N., Chen, P., Lu, W.-J., Pogue, K., Chuong, A., Mata, M., Checketts, J., and Abrams, J.M. (2007). A collective form of cell death requires homeodomain interacting protein kinase. J. Cell Biol. *178*, 567–574.

Lushchak, V.I. (2012). Glutathione homeostasis and functions: potential targets for medical interventions. J. Amino Acids *2012*, 736837.

Markstein, M., Pitsouli, C., Villalta, C., Celniker, S.E., and Perrimon, N. (2008). Exploiting position effects and the gypsy retrovirus insulator to engineer precisely expressed transgenes. Nat. Genet. *40*, 476.

Mount, S.M. (1987). Sequence similarity. Nature *325*, 487.

Nakahira, K., Haspel, J.A., Rathinam, V.A., Lee, S.-J., Dolinay, T., Lam, H.C., Englert, J.A., Rabinovitch, M., Cernadas, M., and Kim, H.P. (2011). Autophagy proteins regulate innate immune responses by inhibiting the release of mitochondrial DNA mediated by the NALP3 inflammasome. Nat. Immunol. *12*, 222.

Nath, A.K., Ryu, J.H., Jin, Y.N., Roberts, L.D., Dejam, A., Gerszten, R.E., and Peterson, R.T. (2015). PTPMT1 inhibition lowers glucose through succinate dehydrogenase phosphorylation. Cell Rep. *10*, 694–701.

Niemi, N.M., Lanning, N.J., Westrate, L.M., and Mackeigan, J.P. (2013). Downregulation of the mitochondrial phosphatase PTPMT1 is sufficient to promote cancer cell death. PLoS One *8*, e53803.

Numata, M., Chu, H.W., Dakhama, A., and Voelker, D.R. (2010). Pulmonary surfactant phosphatidylglycerol inhibits respiratory syncytial virus–induced inflammation and infection. Proc. Natl. Acad. Sci. U S A *107*, 320–325.

Numata, M., Kandasamy, P., Nagashima, Y., Posey, J., Hartshorn, K., Woodland, D., and Voelker, D.R. (2012). Phosphatidylglycerol suppresses influenza A virus infection. Am. J. Respir. Cell Mol. Biol. *46*, 479–487.

Obata, F., Kuranaga, E., Tomioka, K., Ming, M., Takeishi, A., Chen, C.-H., Soga, T., and Miura, M. (2014). Necrosis-driven systemic immune response alters SAM metabolism through the FOXO-GNMT axis. Cell Rep. *7*, 821–833.

Oey, N.A., Ijlst, L., van Roermund, C.W., Wijburg, F.A., and Wanders, R.J. (2005). dif-1 and colt, both implicated in early embryonic development, encode carnitine acylcarnitine translocase. Mol. Genet. Metab. *85*, 121–124.

Pagliarini, D.J., and Dixon, J.E. (2006). Mitochondrial modulation: reversible phosphorylation takes center stage? Trends Biochem. Sci. *31*, 26–34.

Pagliarini, D.J., Wiley, S.E., Kimple, M.E., Dixon, J.R., Kelly, P., Worby, C.A., Casey, P.J., and Dixon, J.E. (2005). Involvement of a mitochondrial phosphatase in the regulation of ATP production and insulin secretion in pancreatic β cells. Mol. Cell *19*, 197–207.

Pagliarini, D.J., Worby, C.A., and Dixon, J.E. (2004). A PTEN-like phosphatase with a novel substrate specificity. J. Biol. Chem. *279*, 38590–38596.

Park, J., Lee, S.B., Lee, S., Kim, Y., Song, S., Kim, S., Bae, E., Kim, J., Shong, M., and Kim, J.-M. (2006). Mitochondrial dysfunction in Drosophila PINK1 mutants is complemented by parkin. Nature *441*, 1157–1161.

Park, Y., Filippov, V., Gill, S.S., and Adams, M.E. (2002). Deletion of the ecdysis-triggering hormone gene leads to lethal ecdysis deficiency. Development *129*, 493–503.

Perkins, L.A., Holderbaum, L., Tao, R., Hu, Y., Sopko, R., McCall, K., Yang-Zhou, D., Flockhart, I., Binari, R., and Shim, H.-S. (2015). The transgenic RNAi project at Harvard Medical School: resources and validation. Genetics *201*, 843–852.

Rongvaux, A., Jackson, R., Harman, C.C., Li, T., West, A.P., de Zoete, M.R., Wu, Y., Yordy, B., Lakhani, S.A., and Kuan, C.-Y. (2014). Apoptotic caspases prevent the induction of type I interferons by mitochondrial DNA. Cell *159*, 1563–1577.

Rosa, J.B., Metzstein, M.M., and Ghabrial, A.S. (2018). An Ichor-dependent apical extracellular matrix regulates seamless tube shape and integrity. PLoS Genet. *14*, e1007146.

Schlame, M., Rüstow, B., Kunze, D., Rabe, H., and Reichmann, G. (1986). Phosphatidylglycerol of rat lung Intracellular sites of formation de novo and acyl species pattern in mitochondria, microsomes and surfactant. Biochem. J. *240*, 247–252.

Scholl, A., O'Brien, M.J., Chandran, R.R., and Jiang, L. (2019). The novel gene apnoia regulates Drosophila tracheal tube size. Dev. Dyn. *248*, 477–487.

Shaukat, Z., Liu, D., and Gregory, S. (2015). Sterile inflammation in Drosophila. Mediators Inflamm. *2015*, 369286.

Shen, J., Liu, X., Yu, W.-M., Liu, J., Nibbelink, M.G., Guo, C., Finkel, T., and Qu, C.-K. (2011). A critical role of mitochondrial phosphatase Ptpmt1 in embryogenesis reveals a mitochondrial metabolic stress-induced differentiation checkpoint in embryonic stem cells. Mol. Cell. Biol. *31*, 4902–4916.

Skouloudaki, K., Papadopoulos, D.K., Tomancak, P., and Knust, E. (2019). The apical protein Apnoia interacts with Crumbs to regulate tracheal growth and inflation. PLoS Genet. *15*, e1007852.

Swanson, L.E., Yu, M., Nelson, K.S., Laprise, P., Tepass, U., and Beitel, G.J. (2009). Drosophila convoluted/dALS is an essential gene required for tracheal tube morphogenesis and apical matrix organization. Genetics *181*, 1281–1290.

Tang, H. (2009). Regulation and function of the melanization reaction in Drosophila. Fly *3*, 105–111.

Tang, H., Kambris, Z., Lemaitre, B., and Hashimoto, C. (2006). Two proteases defining a melanization cascade in the immune system of Drosophila. J. Biol. Chem. *281*, 28097–28104.

Tang, H., Kambris, Z., Lemaitre, B., and Hashimoto, C. (2008). A serpin that regulates immune melanization in the respiratory system of Drosophila. Dev. Cell *15*, 617–626.

Teh, P.G., Chen, M.J., Engel, J.L., Worby, C.A., Manning, G., Dixon, J.E., and Zhang, J. (2013). Identification of a mammalian-type phosphatidylglycerophosphate phosphatase in the Eubacterium *Rhodopirellula baltica*. J. Biol. Chem. *288*, 5176–5185.

Thibault, S.T., Singer, M.A., Miyazaki, W.Y., Milash, B., Dompe, N.A., Singh, C.M., Buchholz, R., Demsky, M., Fawcett, R., and Francis-Lang, H.L. (2004). A complementary transposon tool kit for *Drosophila melanogaster* using P and piggyBac. Nat. Genet. *36*, 283–287.

Tsai, P.-I., Lin, C.-H., Hsieh, C.-H., Papakyrikos, A.M., Kim, M.J., Napolioni, V., Schoor, C., Couthouis, J., Wu, R.-M., and Wszolek, Z.K. (2018). PINK1 phosphorylates MIC60/Mitofilin to control structural plasticity of mitochondrial crista junctions. Mol. Cell *69*, 744–756.e6.

Tsai, P.-I., Papakyrikos, A.M., Hsieh, C.-H., and Wang, X. (2017). Drosophila MIC60/mitofilin conducts dual roles in mitochondrial motility and crista structure. Mol. Biol. Cell *28*, 3471–3479.

Tzou, P., Ohresser, S., Ferrandon, D., Capovilla, M., Reichhart, J.-M., Lemaitre, B., Hoffmann, J.A., and Imler, J.-L. (2000). Tissue-specific inducible expression of antimicrobial peptide genes in Drosophila surface epithelia. Immunity *13*, 737–748.

Wagner, C., Isermann, K., and Roeder, T. (2009). Infection induces a survival program and local remodeling in the airway epithelium of the fly. FASEB J. *23*, 2045–2054.

West, A.P., Khoury-Hanold, W., Staron, M., Tal, M.C., Pineda, C.M., Lang, S.M., Bestwick, M., Duguay, B.A., Raimundo, N., and MacDuff, D.A. (2015). Mitochondrial DNA stress primes the antiviral innate immune response. Nature *520*, 553–557.

White, M.J., McArthur, K., Metcalf, D., Lane, R.M., Cambier, J.C., Herold, M.J., van Delft, M.F., Bedoui, S., Lessene, G., and Ritchie, M.E. (2014). Apoptotic caspases suppress mtDNA-induced STING-mediated type I IFN production. Cell *159*, 1549–1562.

Xiao, J., Engel, J.L., Zhang, J., Chen, M.J., Manning, G., and Dixon, J.E. (2011). Structural and functional analysis of PTPMT1, a phosphatase required for cardiolipin synthesis. Proc. Natl. Acad. Sci. U S A *108*, 11860–11865.

Xu, Q.-Y., Deng, P., Mu, L.-L., Fu, K.-Y., Guo, W.-C., and Li, G.-Q. (2019). Silencing Taiman impairs larval development in *Leptinotarsa decemlineata*. Pestic. Biochem. Physiol. *160*, 30–39.

Xu, Y., Condell, M., Plesken, H., Edelman-Novemsky, I., Ma, J., Ren, M., and Schlame, M. (2006). A Drosophila model of Barth syndrome. Proc. Natl. Acad. Sci. U S A *103*, 11584–11588.

Yu, W.-M., Liu, X., Shen, J., Jovanovic, O., Pohl, E.E., Gerson, S.L., Finkel, T., Broxmeyer, H.E., and Qu, C.-K. (2013). Metabolic regulation by the mitochondrial phosphatase PTPMT1 is required for hematopoietic stem cell differentiation. Cell Stem Cell *12*, 62–74.

Yue, X.Z., Li, D., Lv, J., Liu, K., Chen, J., and Zhang, W.Q. (2019). Involvement of mind the gap in the organization of the tracheal apical extracellular matrix in *Drosophila* and *Nilaparvata lugens*. Insect Sci. *27*, 756–770.

Zhang, J., Guan, Z., Murphy, A.N., Wiley, S.E., Perkins, G.A., Worby, C.A., Engel, J.L., Heacock, P., Nguyen, O.K., and Wang, J.H. (2011). Mitochondrial phosphatase PTPMT1 is essential for cardiolipin biosynthesis. Cell Metab. *13*, 690–700.

Zheng, H., Yu, W.-M., Shen, J., Kang, S., Hambardzumyan, D., Li, J.Y., Shen, Y., Kenney, A.M., Chen, J., and Qu, C.-K. (2018). Mitochondrial oxidation of the carbohydrate fuel is required for neural precursor/stem cell function and postnatal cerebellar development. Sci. Adv. *4*, eaat2681.

Zhou, R., Yazdi, A.S., Menu, P., and Tschopp, J. (2011). A role for mitochondria in NLRP3 inflammasome activation. Nature *469*, 221–225.

iScience, Volume *23*

Supplemental Information

Drosophila PTPMT1 Has a Function in Tracheal Air Filling

Amanda M. Papakyrikos, Min Joo Kim, and Xinnan Wang

Figure S1

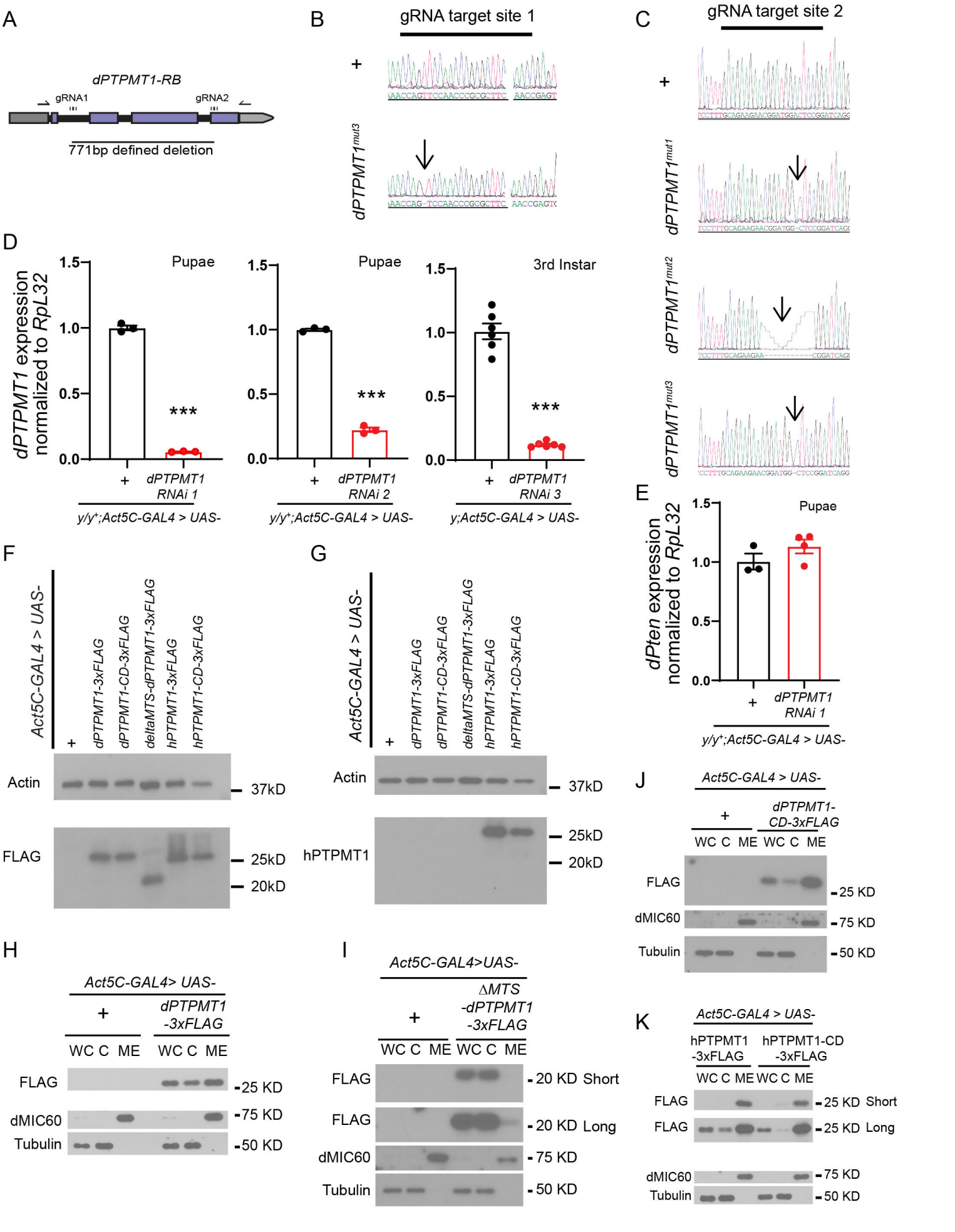
A
dPTPMT1-RB
gRNA1
gRNA2
771bp defined deletion
B
gRNA target site 1
+
dPTPMT1mut3
C
gRNA target site 2
+
dPTPMT1mut1
dPTPMT1mut2
dPTPMT1mut3
D
dPTMT1 expression normalized to RpL32
Pupae
Pupae
3rd Instar
***
+
dPTPMT1 RNAi 1
dPTPMT1 RNAi 2
dPTPMT1 RNAi 3
y/y+;Act5C-GAL4 > UAS-
y/y+;Act5C-GAL4 > UAS-
y;Act5C-GAL4 > UAS-
E
dPten expression normalized to RpL32
Pupae
+
dPTPMT1 RNAi 1
y/y+;Act5C-GAL4 > UAS-
F
Act5C-GAL4 > UAS-
+
dPTPMT1-3xFLAG
dPTPMT1-CD-3xFLAG
deltaMTS-dPTPMT1-3xFLAG
hPTPMT1-3xFLAG
hPTPMT1-CD-3xFLAG
Actin
37kD
FLAG
25kD
20kD
G
Act5C-GAL4 > UAS-
+
dPTPMT1-3xFLAG
dPTPMT1-CD-3xFLAG
deltaMTS-dPTPMT1-3xFLAG
hPTPMT1-3xFLAG
hPTPMT1-CD-3xFLAG
Actin
37kD
hPTPMT1
25kD
20kD
H
Act5C-GAL4> UAS-
+
dPTPMT1 -3xFLAG
WC C ME WC C ME
FLAG
25 KD
dMIC60
75 KD
Tubulin
50 KD
I
Act5C-GAL4>UAS-
+
ΔMTS -dPTPMT1 -3xFLAG
WC C ME WC C ME
FLAG
20 KD Short
FLAG
20 KD Long
dMIC60
75 KD
Tubulin
50 KD
J
Act5C-GAL4 > UAS-
+
dPTPMT1-CD-3xFLAG
WC C ME WC C ME
FLAG
25 KD
dMIC60
75 KD
Tubulin
50 KD
K
Act5C-GAL4 > UAS-
hPTPMT1 -3xFLAG
hPTPMT1-CD -3xFLAG
WC C ME WC C ME
FLAG
25 KD Short
FLAG
25 KD Long
dMIC60
75 KD
Tubulin
50 KD

Figure S2

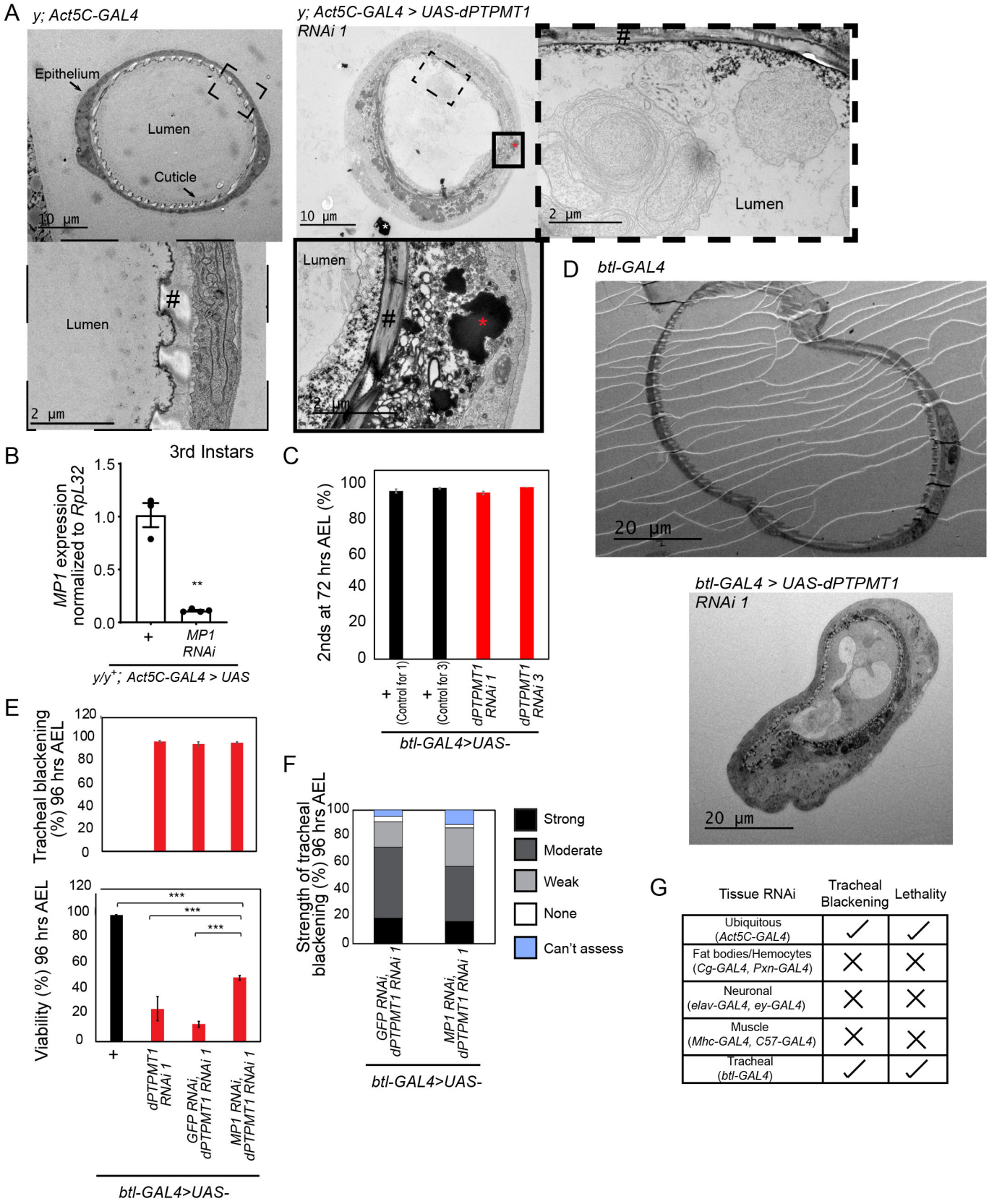
A
y; Act5C-GAL4
Epithelium
Lumen
Cuticle
10 µm
Lumen
#
2 µm
y; Act5C-GAL4 > UAS-dPTPMT1 RNAi 1
10 µm
#
2 µm
Lumen
Lumen
#
2 µm
B
3rd Instars
MP1 expression normalized to RpL32
1.5
1.0
0.5
0.0
**
+
MP1 RNAi
y/y+; Act5C-GAL4 > UAS
C
2nds at 72 hrs AEL (%)
100
80
60
40
20
0
+ (Control for 1)
+ (Control for 3)
dPTPMT1 RNAi 1
dPTPMT1 RNAi 3
btl-GAL4>UAS-
D
btl-GAL4
20 µm
btl-GAL4 > UAS-dPTPMT1 RNAi 1
20 µm
E
Tracheal blackening (%) 96 hrs AEL
120
100
80
60
40
20
0
Viability (%) 96 hrs AEL
120
100
80
60
40
20
0
***
***
***
+
dPTPMT1 RNAi 1
GFP RNAi; dPTPMT1 RNAi 1
MP1 RNAi; dPTPMT1 RNAi 1
btl-GAL4>UAS-
F
Strength of tracheal blackening (%) 96 hrs AEL
100
80
60
40
20
0
Strong
Moderate
Weak
None
Can't assess
GFP RNAi; dPTPMT1 RNAi 1
MP1 RNAi; dPTPMT1 RNAi 1
btl-GAL4>UAS-
G
Tissue RNAi
Tracheal Blackening
Lethality
Ubiquitous (Act5C-GAL4)
Fat bodies/Hemocytes (Cg-GAL4, Pxn-GAL4)
Neuronal (elav-GAL4, ey-GAL4)
Muscle (Mhc-GAL4, C57-GAL4)
Tracheal (btl-GAL4)

Figure S3

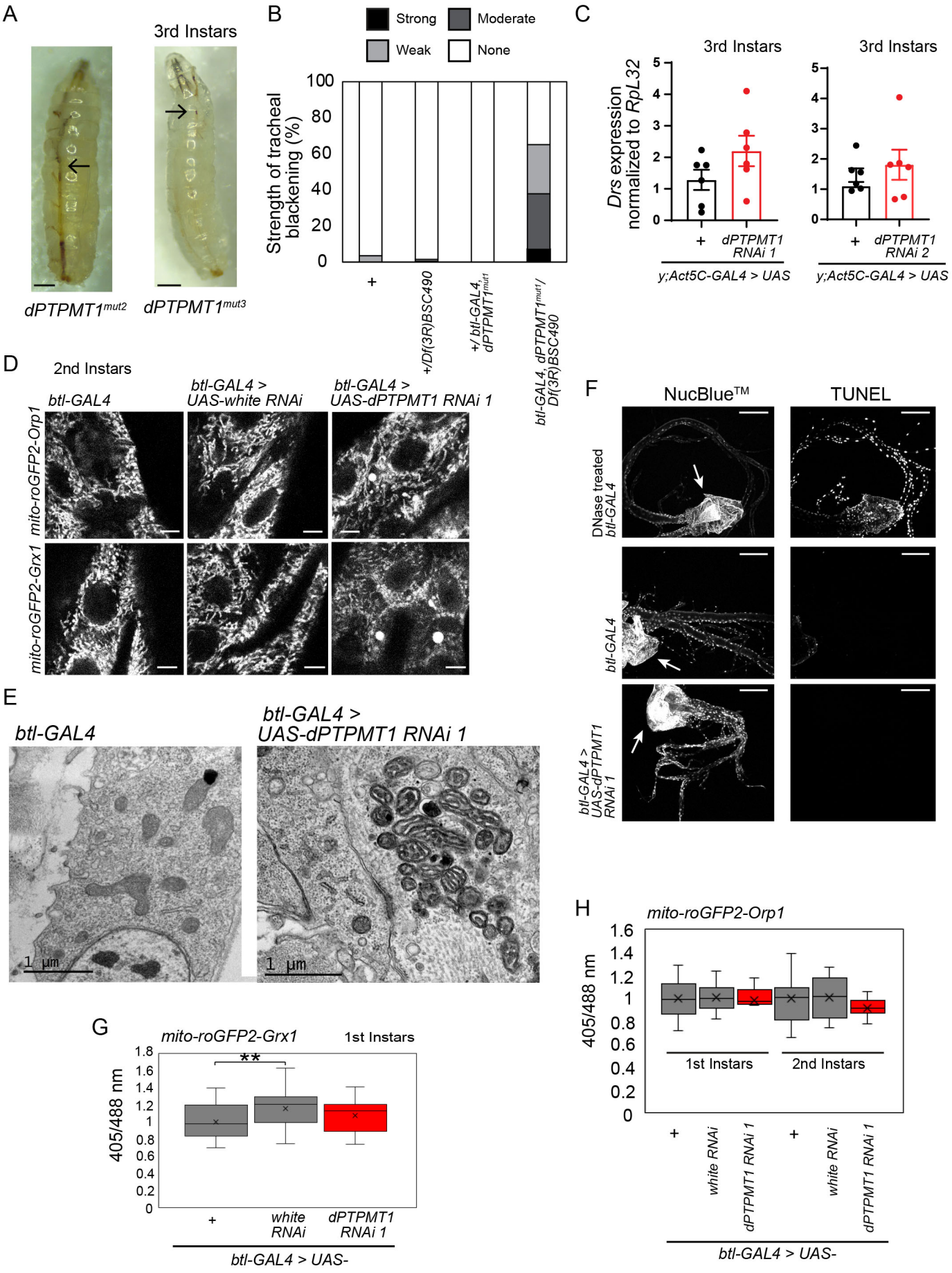
A
3rd Instars
dPTPMT1mut2
dPTPMT1mut3
B
Strong
Moderate
Weak
None
Strength of tracheal blackening (%)
100
80
60
40
20
0
+
+/Df(3R)BSC490
+/ btl-GAL4, dPTPMT1mut1
btl-GAL4, dPTPMT1mut1 / Df(3R)BSC490
C
3rd Instars
3rd Instars
Drs expression normalized to RpL32
5
4
3
2
1
0
+
dPTPMT1 RNAi 1
dPTPMT1 RNAi 2
y;Act5C-GAL4 > UAS
y;Act5C-GAL4 > UAS
D
2nd Instars
btl-GAL4
btl-GAL4 > UAS-white RNAi
btl-GAL4 > UAS-dPTPMT1 RNAi 1
mito-roGFP2-Orp1
mito-roGFP2-Grx1
E
btl-GAL4
btl-GAL4 > UAS-dPTPMT1 RNAi 1
1 µm
1 µm
F
NucBlue™
TUNEL
DNase treated btl-GAL4
btl-GAL4
btl-GAL4 > UAS-dPTPMT1 RNAi 1
G
mito-roGFP2-Grx1
1st Instars
405/488 nm
1.8
1.6
1.4
1.2
1
0.8
0.6
0.4
0.2
0
**
+
white RNAi
dPTPMT1 RNAi 1
btl-GAL4 > UAS-
H
mito-roGFP2-Orp1
405/488 nm
1.6
1.4
1.2
1
0.8
0.6
0.4
0.2
0
1st Instars
2nd Instars
+
white RNAi
dPTPMT1 RNAi 1
+
white RNAi
dPTPMT1 RNAi 1
btl-GAL4 > UAS-

Figure S4

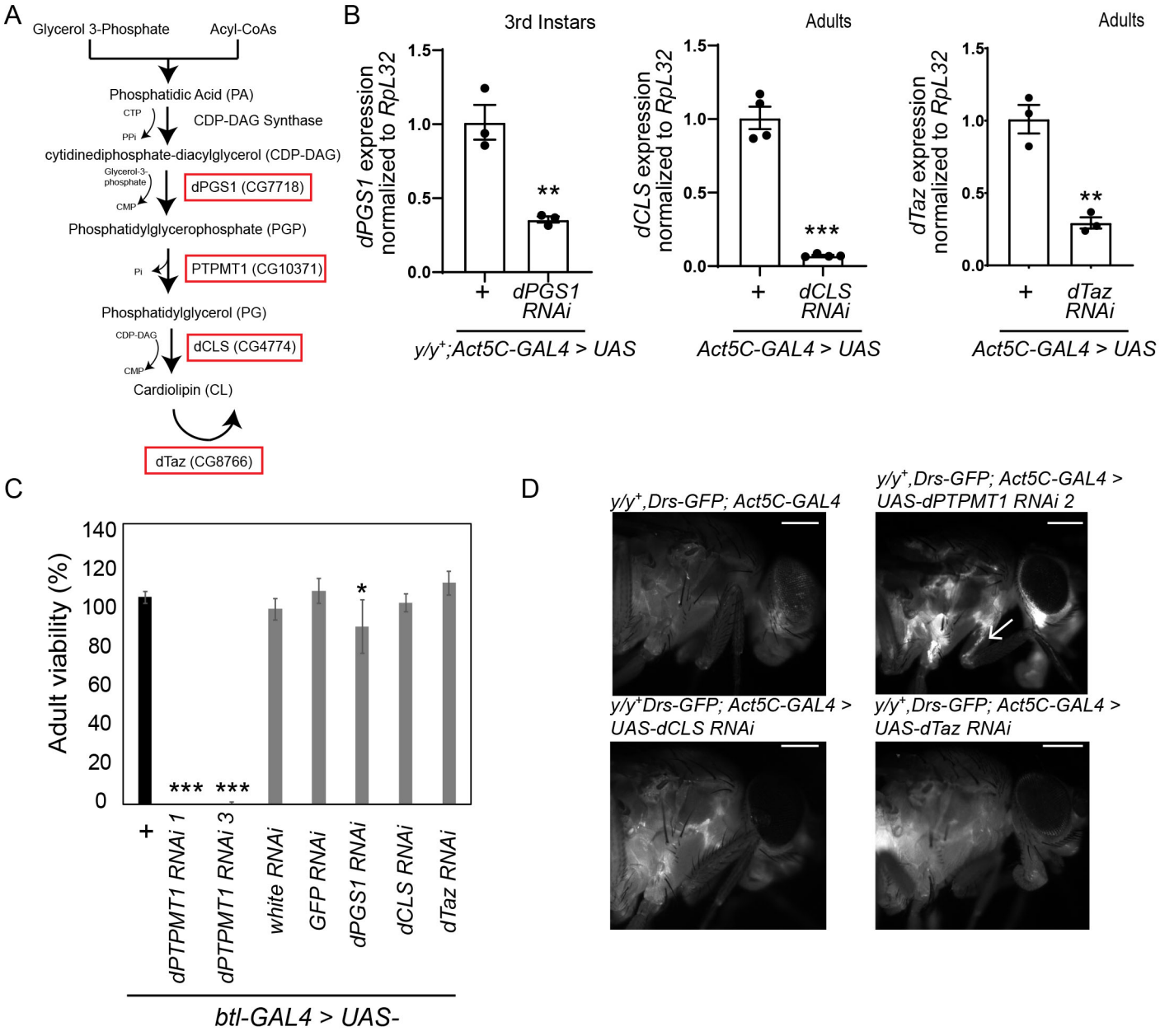
A
Glycerol 3-Phosphate
Acyl-CoAs
Phosphatidic Acid (PA)
CTP
PPi
CDP-DAG Synthase
cytidinediphosphate-diacylglycerol (CDP-DAG)
Glycerol-3-phosphate
CMP
dPGS1 (CG7718)
Phosphatidylglycerophosphate (PGP)
Pi
PTPMT1 (CG10371)
Phosphatidylglycerol (PG)
CDP-DAG
CMP
dCLS (CG4774)
Cardiolipin (CL)
dTaz (CG8766)
B
3rd Instars
dPGS1 expression normalized to RpL32
1.5
1.0
0.5
0.0
**
+
dPGS1 RNAi
y/y+;Act5C-GAL4 > UAS
Adults
dCLS expression normalized to RpL32
***
dCLS RNAi
Act5C-GAL4 > UAS
Adults
dTaz expression normalized to RpL32
dTaz RNAi
Act5C-GAL4 > UAS
C
Adult viability (%)
140
120
100
80
60
40
20
0
***
***
*
+
dPTPMT1 RNAi 1
dPTPMT1 RNAi 3
white RNAi
GFP RNAi
dPGS1 RNAi
dCLS RNAi
dTaz RNAi
btl-GAL4 > UAS-
D
y/y+,Drs-GFP; Act5C-GAL4
y/y+,Drs-GFP; Act5C-GAL4 > UAS-dPTPMT1 RNAi 2
y/y+Drs-GFP; Act5C-GAL4 > UAS-dCLS RNAi
y/y+,Drs-GFP; Act5C-GAL4 > UAS-dTaz RNAi

SUPPLEMENTARY FIGURE LEGENDS

Figure S1. Generation of *dPTPMT1* Mutants and Transgenes, Related to Figure 1. (A) Design for CRISPR-mutagenesis. Exons of *dPTPMT1* transcript are indicated with wide purple bars and introns with black lines. *vas-Cas9*-expressing embryos were injected with two guide RNAs (dashed lines) in order to create a defined deletion. Locations of primers for screening are indicated with half arrows. (B-C) The direct sequencing chromatograms of $dPTPMT1^{mut}$ lines are shown. Arrows point to deletions. $dPTPMT1^{mut3}$ has a 1 bp deletion within the first gRNA site (B). $dPTPMT1^{mut1-3}$ have deletions in the second gRNA site (C). (D-E) qPCR evaluation of *dPTPMT1* (D) or *dPten* (E) transcript levels. Pupae were mixed-sex, females are heterozygous for *y* and males are hemizygous for *y*. n=3-6 replicates, 15-20 pupae for each repeat (RNAi 1&2) or 3rd instar males (RNAi 3). Data are represented as mean ± SEM and *** $p<0.001$, by one-tailed Student's t-test. (F-G) Validation of *PTPMT1* transgene expression. Whole fly lysates of 0- to 2-day-old adults were immunoblotted with the antibodies indicated. (H-K) Cellular localization of ubiquitously expressed *dPTPMT1-3×FLAG* (H), Δ*MTS-dPTPMT1-3×FLAG* (I), *dPTPMT1-CD-3×FLAG* (J), *hPTPMT1-3×FLAG* and *hPTPMT1-CD-3×FLAG* (K). Whole cell fraction (WC), cytosolic fraction (C), mitochondrial-enriched fraction (ME) were prepared and immunoblotted with the antibodies indicated. Results were observed 3 times and representative blots are shown. Equal total protein from each fraction was loaded. "Short" = short exposure, "Long" = long exposure.

Figure S2. **dPTPMT1 Depletion Results in Tracheal Blackening and Lethality, Related to Figure 2.** (A) TEM images of transverse sections of the dorsal trunk of the trachea in a 3rd instar male with ubiquitous *dPTPMT1* RNAi. Cuticle indicated by the # symbol. Red asterisk indicates electron dense regions. White asterisk indicates dust on the thin section. Dashed boxes show higher

magnifications of key areas. Scale bars (low magnification), 10 μm, scale bars (high magnification), 2 μm. (B) qPCR validation of *MP1* RNAi. Pupae were mixed-sex, females are heterozygous for *y* and males are hemizygous for *y*. n= 3-4 replicates, 20 for each repeat. Data are represented as mean ± SEM and ** $p < 0.01$, by one-tailed Student's t-test. (C) Percentage of larvae at 72 hours AEL which are 2nd instars, in tracheal-specific *dPTPMT1* RNAi. n=2-3 replicates, 40-94 for each repeat. Data are represented as mean ± SEM and $p > 0.05$, by Chi-square test. (D) TEM images of transverse sections of the dorsal trunk of the trachea in a 3rd instar male with tracheal-specific *dPTPMT1* RNAi and a control larva. Note the collapsed trachea and electron dense lumen in the mutant. Crosses were grown at 25ºC for three days and then shifted to 30ºC to drive a stronger knockdown. Scale bars, 20 μm. (E) Percentage of larvae with tracheal blackening and viability in tracheal-specific RNAi of *MP1* and *dPTPMT1*. n=2-3 replicates, 54-100 for each repeat. Control data (left two bars) is the same as in Figure 2F. Data are represented as mean ± SEM and *** $p < 0.001$, by Chi-square test. (F) Strength of tracheal blackening in tracheal-specific RNAi of *MP1* and *dPTPMT1*. n=179-199 larvae, 2 independent crosses. (G) Screen for phenotypes following tissue-specific *dPTPMT1* RNAi. Crosses were grown at 25ºC for three days and then shifted to 30ºC to drive a stronger knockdown.

Figure S3. dPTPMT1 Depletion Results in Tracheal Blackening, *Drs* Upregulation, and Mitochondrial Defects, Related to Figure 2, Figure 3, and Figure 4. (A) $dPTPMT1^{mut2}$ and $dPTPMT1^{mut3}$ mutants show tracheal blackening. Scale, 250 μm. (B) Strength of tracheal blackening in $dPTPMT1^{mut1}$ 3rd instar larvae. n=81-226, 3-4 independent crosses. (C) qPCR evaluation of *Drs* expression in 3rd instar male larvae with ubiquitous *dPTPMT1* RNAi. n=6 replicates, 20 for each repeat. Data are represented as mean ± SEM and $p > 0.05$, by one-tailed

Student's t-test. (D) Enlarged mito-roGFP puncta visualized by live imaging mitochondrially localized ROS reporters in tracheal epithelial cells of 2nd instars with tracheal-specific *dPTPMT1* RNAi. Scale, 5 μm. (E) TEM images show a cluster of mitochondria in a 3rd instar male larva with tracheal-specific *dPTPMT1* RNAi. Crosses were grown at 25ºC for three days and then shifted to 30ºC to drive a stronger knockdown. Scale, 1 μm. (F) TUNEL staining of the tracheae of 2nd instar larvae. NucBlue™ stains nuclei. Arrows point to the larval cuticle. DNase treatment causes double strand breaks (top row), serving as a positive control. Percentage of TUNEL positive nuclei: *btl-GAL4* (Control for RNAi 1): 1% ±1%, *btl-GAL4>UAS-dPTPMT1* RNAi 1: 2% ±1%, *btl-GAL4>UAS-GFP* RNAi: 3% ±1%, *btl-GAL4* (Control for RNAi 3): 1% ±1%, *btl-GAL4>UAS-dPTPMT1* RNAi 3: 1% ±1%. n=8-18 larvae, 2 independent crosses. Scale, 100 μm. Data are represented as mean ± SEM and $p > 0.05$, by one-tailed Student's t-test. (G-H) Quantification of the fluorescence ratios of mitochondrially localized roGFP-Grx1 (G) and roGFP2-Orp1 (H) expressed in the trachea of 2nd instars. n=8-30. Boxes show 25th/75th percentiles, whiskers are the minimum and maximum values, and x is the median marker and ** $p < 0.01$, by one-tailed Student's t-test.

Figure S4. **Mutants of the CL Pathway Do not Mimic Phenotypes of *dPTPMT1* Deficiency, Related to Figure 4.** (A) Biosynthesis of cardiolipin, inspired by Zhang et al. 2011. (B) qPCR data for RNAi of enzymes in CL biosynthesis. n=3-4 replicates, 20 for each repeat. *dCLS* = adults females, 0-2 days old. *dTaz* = half male and half female adults, 0-2 days old. *dPGS1* = 3rd instar larvae, mixed sex, females are heterozygous for *y* and males are hemizygous for *y*. Data are represented as mean ± SEM and ** $p < 0.01$, *** $p < .001$ by one-tailed Student's t-test. (C) Viability of tracheal RNAi of CL pathway enzymes. n=3 replicates. 0- to 2-day-old adults. Crosses

were grown at 25ºC for three days and then shifted to 30ºC to drive a stronger knockdown. For simplicity only one background control is shown. Genotypic frequency is calculated for the genotype of interest and then normalized to its expected genotypic frequency. Statistical significance is given relative to respective controls. *dPGS1* RNAi viability was significantly decreased relative to its control. Data are represented as mean ± SEM and * $p<0.05$, *** $p<0.001$ by Chi-square test. (D) *Drs-GFP* expression in females with ubiquitous RNAi of *dTaz* and *dCLS*. Control images and ubiquitous *dPTPMT1* RNAi are the same as in Figure 3C. Scale, 250 μm.

TRANSPARENT METHODS

EXPERIMENTAL MODEL AND SUBJECT DETAILS

Fly Stocks

dPTPMT1 (CG10371) RNAi stocks included *UAS-dPTPMT1* RNAi 1(VDRC 47624GD), *UAS-dPTPMT1* RNAi 2 (VDRC 47623GD), *UAS-dPTPMT1* RNAi 3 (BDSC 40913). For *dPTPMT1* RNAi controls, drivers were crossed to background controls specific to the RNAi line used. For *dPTPMT1* RNAi 1 and 2 controls ("Control for 1&2"), drivers were crossed to VDRC 60000GD. For *dPTPMT1* RNAi 3 controls ("Control for 3"), drivers were crossed to BDSC 36303. Additional RNAi stocks included *UAS-dPGS1* RNAi (VDRC 109405KK), *UAS-dCLS* RNAi (BDSC 77150), *UAS-dTaz* RNAi (BDSC 31099), *UAS-GFP* RNAi (BDSC 41557), *UAS-white* RNAi (a gift from Dr. Bingwei Lu's Lab), and *UAS-MP1* RNAi (VDRC 18970GD). BDSC 36303 was used as a background control for *dCLS*, *dTaz*, and *MP1* RNAi experiments. VDRC 60100KK was used as a background control for *dPGS1* RNAi. Additional stocks included *y, Drs-GFP* (BDSC 55707), *UAS-mito-HA-GFP* (BDSC 8442), *UAS-mito-roGFP2-Orp1* (BDSC 67667), *UAS-mito-roGFP2-*

Grx1 (BDSC 67664), *btl-GAL4* (BDSC 78328, the *y* background mutation was removed by outcrossing), *y,w*;*Act5C-GAL4* (Wang lab stock), *C57-GAL4* (Wang lab stock), *Mhc-GAL4* (Wang lab stock), *ey-GAL4* (a gift from Dr. Bingwei Lu's Lab), *elav-GAL4* (BDSC 458, a gift from Liqun Luo Lab), *Cg-GAL4* (BDSC 7011), *Pxn-GAL4* (a gift from Dr. Clarissa Cheney Lab), *Df(3R)BSC490* (BDSC 24994), *Df(3R)Exel9013* (BDSC 7991), *vas-Cas9* (BDSC 51323), *dCLS* mutants (BDSC 17917, BDSC 10741) (Thibault et al., 2004), $Pink1^{rv}$ (Park et al., 2006), and $Pink1^{B9}$ (Park et al., 2006), $dMIC60^{mut}$ (Tsai et al., 2017), *e/TM3* (*ActGFP, ser*) (BDSC 7408), and *Dr/TM6B* (Wang Lab stock).

Flies were grown on a standard molasses media except where otherwise stated in the methods. For *Act5C-GAL4*-driven crosses, flies were grown at 25ºC for 3 days and then switched to 30ºC to drive a stronger knockdown. In all other experiments, flies were maintained at 25ºC, except where otherwise stated in the figure legends. Because there is evidence that the presence of yellow mutations (*y*) impact immune phenotypes (Tang et al., 2008), we indicated the presence of this mutation in all experiments. Developmental stage, age, and sex of samples are given in the figure legends. All adults were between 0-2 days old, except for the *Pink11* mutants which were aged to 5 days and the adult flies used for mitochondrial enrichments, which were 1-3 days old. Where possible, we used males in our assessments of adult phenotypes, except in the case of adults on a *Drs-GFP* background, as males in this background showed reduced viability. For qPCR on adults, we used equal ratios of males and females, except for *dCLS* RNAi where we used females only because males had reduced viability. Additionally, for the assessment of *Drs* levels in adults with ubiquitous *dPTPMT1* RNAi, we used males only in order to control for the presence of yellow mutations in this background. Between 1-376 adults were used for each genotype in each experiment. Between 1-699 larvae were used for each genotype in each experiment.

METHOD DETAILS

CRISPR/Cas9: *dPTPMT1* mutants were generated using the methods of the O'Connor-Giles, Wildonger, and Harrison labs (Gratz et al., 2013, Gratz et al., 2015) for creating defined deletions. Transgenic flies expressing Cas9 protein in their ovaries under the control of *vas* regulatory sequences (BDSC 51323) were sequenced for SNPs. Two gRNAs (gRNA1 5'-CTTCGTTGAAGCGCGGGTTGGAAC-3', gRNA2 5'-CTTCGCAGAAGAACGGATGGACTC-3') were identified using the flyCRISPR Optimal Target Finder (http://tools.flycrispr.molbio.wisc.edu/targetFinder/). These gRNAs would be expected to generate a defined deletion of ~770bp. gRNAs were selected in regions that did not contain SNPs and did not overlap with neighboring genes. gRNAs were cloned into pU6-BbsI-chiRNA using restriction-enzyme cloning (Gratz et al., 2013). pU6-BbsI-chiRNA was a gift from Melissa Harrison, Kate O'Connor-Giles, and Jill Wildonger (Addgene plasmid # 45946; http://n2t.net/addgene:45946; RRID:Addgene_45946). gRNA oligonucleotides were designed with a 4bp overhang complementary to those generated by BbsI (see above). Oligonucleotides were purchased pre-phosphorylated from Integrated DNA Technologies (Redwood City, CA) and were subsequently annealed at 95 ^{o}C for 5 minutes in T4 ligation buffer (NEB, B0202S). pU6-BbsI-chiRNA was digested with BbsI (NEB, R0539S), dephosphorylated with Calf Intestinal Alkaline Phosphatase (NEB, M0290), and then ligated with oligonucleotides using T4 DNA ligase (NEB, M0202S). The resulting constructs were midi-prepped and sequenced by Genewiz (South San Francisco, CA) using T3 and T7 primers (5'-GCAATTAACCCTCACTAAAGG-3', 5'-TAATACGACTCACTATAGGG-3'). gRNAs were injected into Cas9 transgenic flies by the BestGene Inc. (Chino Hills, CA) at 100 ng/µl and 250 ng/µl per plasmid. Progeny from injections

were kept at 18ºC for the duration of the screen, in order to promote survival of weak *dPTPMT1* mutants. F0s were crossed to *Dr/TM6B* balancer flies (Wang Lab Stock) in order to create stable F2 stocks. Homozygous lethal F2 lines were screened over deficiency lines covering PTPMT1 (BDSC 24994, BDSC 7991). Homozygous larvae, from stocks which were lethal over deficiency lines, were sequenced for mutations in *dPTPMT1*. The *dPTPMT1* gene region was amplified by PCR (5'-GTTATGCAAAGGAACGCGCA-'3, 5'-CGTAACAAAGGTGGTGCCTG-'3). PCR products were gel-extracted using the QIAquick Gel Extraction Kit (Qiagen, 28706) and sent for sequencing.

Fly DNA preparations and polymerase chain reaction (PCR): A single larva was manually crushed in 50-100 µl of fly squishing buffer (FSB: 10mM Tris-HCl pH8, 1mM EDTA, 25mM NaCl) and 0.2 mg/ml of Proteinase K (NEB, P8107S). Lysates were incubated at 37ºC for 30 minutes and then boiled for 10 minutes at 95ºC to inactivate the Proteinase K. PCR reactions were performed using 1-4 µl of crude DNA. Platinum™ Green Hot Start PCR Master Mix (2X) (Thermo Fischer, 13001012) or Q5® High-Fidelity 2X Master Mix (NEB, M0492S) were used for PCR reactions, following manufacturer's instructions.

Quantitative real-time PCR (qPCR): Total RNA was extracted by homogenization in TRIzol (Thermo Fisher, 15596026) and then mixed with chloroform vigorously and centrifuged at 12,000g at 4°C for 15 minutes. To precipitate the RNA, the aqueous phase was mixed with 100% isopropanol at 1:1 ratio. RNA pellets were washed with 70% ethanol and then resuspended in nuclease-free water. RNA was cleaned with chloroform (1:1), vortexed, and then centrifuged at 10,000g at 4°C. The aqueous phase was removed and mixed with ice-cold ethanol (1:3) and sodium

acetate (pH 4.8, 10:1) and precipitated overnight at -20°C. The RNA pellet was washed in 70% ethanol, dried, and then resuspended in DNase, RNase free water. To remove DNA contamination, RNA was treated with DNase (NEB, M0303S), following manufacturer's instructions. cDNA synthesis was performed with iScript Reverse Transcription Supermix (Bio-RAD, 1708841) using 500 ng of DNase-treated RNA. cDNA was diluted by 4.5-fold with DNase/RNase free water for qPCR. qPCR was performed using Taqman Fast Advanced Master Mix (Applied Biosystems, 4444557) and commercially available TaqMan Gene Expression Assay probes (Applied Biosystems: *Drs*: Dm01822006_s1, *MP1*:Dm02136644_g1, *dPTPMT1*:Dm02143827_g1, *RpL32RpL32*:Dm02151827_g1, *dPten*:Dm01844965_g1, *dCLS*:Dm02144883_g1, *dTaz*:Dm01793307_g1, *dPGS*1: Dm02142030_g1) and analyzed by a Step One Plus Real-Time PCR System (Applied Biosystems) following manufacturer's instructions. Analysis was performed using the ΔΔCT method (Livak and Schmittgen, 2001). Expression was normalized to the house-keeping gene *RpL32*. A minimum of 3 replicates were performed for each experiment. For qPCR evaluation of *Drs* expression, individuals were collected at the same time of day, to control for possible circadian variation in expression of immune genes, as recommended by others (Neyen et al., 2014).

Generation of *dPTPMT1* transgenic flies: pUASTattB-dPTPMT1-3×FLAG, pUASTattB-ΔMTS-dPTPMT1-3×FLAG and pUASTattB-hPTPMT1-3×FLAG were generated by GenScript (Piscataway, NJ). WT *dPTPMT1* (isoform RB), Δ*1-31-dPTPMT1*, and codon optimized *hPTPMT1* (isoform 1) were synthesized by GenScript (Piscataway, NJ) and cloned into pUASTattB (Groth et al., 2004) using NotI/XbaI. A modified kozak sequence was added to the 5' end (Pfeiffer et al., 2012) to enhance gene expression and a codon-optimized 3×FLAG tag was added to the 3' end to

facilitate localization studies. Site-directed mutagenesis, performed by GenScript, was used to generate pUASTattB-dPTPMT1-CD-3×FLAG and pUASTattB-hPTPMT1-CD-3×FLAG. We used PhiC31 integrase-mediated transgenesis to generate transgenic fly lines (Markstein et al., 2008). All constructs were injected by the Bestgene Inc (Chino Hills, CA) into y^{1}, w^{67c23}; P{CaryP}attP40 flies (the Bestgene Inc), with an estimated insertion at 25C6 (Markstein et al., 2008).

Inserted sequences for *dPTPMT1* constructs: NotI sequence is in red, XbaI sequence is in blue, modified Kozak (Pfeiffer et al., 2012) is underlined, and 3×FLAG sequence is in bold.

dPTPMT1-3×FLAG **(Isoform RB):**

GCGGCCGCAACTTAAAAAAAAAAATCAAAATGGAGATGAGTGCTGCCATGTTCGCA
CGCGTTTCCTTCTACCCCACCCTGCTGTACAATGTCCTGATGGAAAAGGCATCGGCC
AGGAATTGGTACGATCGCATCGATGAGCATGTGATACTGGGAGCACTGCCCTTTCGC
AGCCAGGCCAATGACCTCATTGAAAAGGAGAACATGAAGGCGGTGGTGTCGATGAA
CGAGGACTATGAGCTGACCGCCTTCTCCAACAACACGGAGAAGTGGCGAAAGCTTG
GCATTGAGTTCCTGCAGCTGGCCACCACCGACATCTTTGAGTCGCCCAATCAAGAAA
AGCTCTTCCGCGGCGTGGAATTCATAAACAAGTTCCTGCCTCTAAAGCAAAGAATTG
GTGGCCTAAGTTCCTCCTACCAGCCGGAGAACGTGGGTTCTGTCTATGTGCACTGCA
AGGCTGGTAGGACGCGAAGTGCCACTTTGGTGGGATGCTACCTCATGATGAAGAAC
GGATGGACTCCGGATCAGGCGGTTGACCACATGCGTAAGTGCCGACCGCACATTCT
GCTGCACACCAAACAATGGGATGCCCTCCGGTTATTCTACACAAACAATGTGGAGA

CGAAATCA**GACTACAAGGATGACGACGATAAGGATTACAAGGATGACGACGAT**

AAGGACTACAAGGATGACGATGATAAGTGATCTAGA

***dPTPMT1-C141S-3×FLAG* (Isoform RB)**:

GCGGCCGCAACTTAAAAAAAAAAATCAAAATGGAGATGAGTGCTGCCATGTTCGCA

CGCGTTTCCTTCTACCCCACCCTGCTGTACAATGTCCTGATGGAAAAGGCATCGGCC

AGGAATTGGTACGATCGCATCGATGAGCATGTGATACTGGGAGCACTGCCCTTTCGC

AGCCAGGCCAATGACCTCATTGAAAAGGAGAACATGAAGGCGGTGGTGTCGATGAA

CGAGGACTATGAGCTGACCGCCTTCTCCAACAACACGGAGAAGTGGCGAAAGCTTG

GCATTGAGTTCCTGCAGCTGGCCACCACCGACATCTTTGAGTCGCCCAATCAAGAAA

AGCTCTTCCGCGGCGTGGAATTCATAAACAAGTTCCTGCCTCTAAAGCAAAGAATTG

GTGGCCTAAGTTCCTCCTACCAGCCGGAGAACGTGGGTTCTGTCTATGTGCACAGCA

AGGCTGGTAGGACGCGAAGTGCCACTTTGGTGGGATGCTACCTCATGATGAAGAAC

GGATGGACTCCGGATCAGGCGGTTGACCACATGCGTAAGTGCCGACCGCACATTCT

GCTGCACACCAAACAATGGGATGCCCTCCGGTTATTCTACACAAACAATGTGGAGA

CGAAATCA**GACTACAAGGATGACGACGATAAGGATTACAAGGATGACGACGAT**

AAGGACTACAAGGATGACGATGATAAGTAATCTAGA

Δ*MTS-dPTPMT1-3×FLAG* (Isoform RB):

GCGGCCGCAACTTAAAAAAAAAAATCAAAATGTACGATCGCATCGATGAGCATGTG

ATACTGGGAGCACTGCCCTTTCGCAGCCAGGCCAATGACCTCATTGAAAAGGAGAA

CATGAAGGCGGTGGTGTCGATGAACGAGGACTATGAGCTGACCGCCTTCTCCAACA

ACACGGAGAAGTGGCGAAAGCTTGGCATTGAGTTCCTGCAGCTGGCCACCACCGAC

ATCTTTGAGTCGCCCAATCAAGAAAAGCTCTTCCGCGGCGTGGAATTCATAAACAAG

TTCCTGCCTCTAAAGCAAAGAATTGGTGGCCTAAGTTCCTCCTACCAGCCGGAGAAC

GTGGGTTCTGTCTATGTGCACTGCAAGGCTGGTAGGACGCGAAGTGCCACTTTGGTG

GGATGCTACCTCATGATGAAGAACGGATGGACTCCGGATCAGGCGGTTGACCACAT

GCGTAAGTGCCGACCGCACATTCTGCTGCACACCAAACAATGGGATGCCCTCCGGTT

ATTCTACACAAACAATGTGGAGACGAAATCA**GACTACAAGGATGACGACGATAAG**

GATTACAAGGATGACGACGATAAGGACTACAAGGATGACGATGATAAGTAATC

TAGA

***hPTPMT1-3×FLAG* (Isoform 1):**

GCGGCCGCAACTTAAAAAAAAAAATCAAAATGGCCGCCACCGCCCTGCTGGAGGCC

GGACTGGCCCGCGTGCTGTTTTACCCAACCCTGCTGTATACCCTGTTTCGCGGAAAG

GTGCCCGGACGCGCCCACCGCGATTGGTACCACCGCATCGACCCCACCGTGCTGCTG

GGAGCCCTGCCCCTGCGCTCGCTGACCCGCCAGCTGGTGCAGGATGAGAACGTGCG

CGGCGTGATCACCATGAATGAGGAGTACGAGACGCGCTTCCTGTGCAACTCGTCGC

AGGAGTGGAAGCGCCTGGGAGTGGAGCAGCTGCGCCTGAGCACCGTGGATATGACC

GGCATCCCAACCCTGGACAATCTGCAGAAGGGCGTGCAGTTCGCCCTGAAGTACCA

GTCCCTGGGCCAGTGCGTGTACGTGCACTGCAAGGCCGGACGCTCGCGCAGCGCCA

CGATGGTGGCCGCCTACCTGATCCAGGTGCACAAGTGGTCCCCAGAGGAGGCCGTG

CGCGCCATTGCCAAGATCCGCTCGTACATTCACATTCGCCCGGGACAGCTGGATGTG

CTGAAGGAGTTCCACAAGCAGATCACCGCCCGCGCCACCAAGGATGGAACCTTCGT

GATCTCCAAGACC**GACTACAAGGATGACGACGATAAGGATTACAAGGATGACGA**

CGATAAGGACTACAAGGATGACGATGATAAGTGATCTAGA

***hPTPMT1-C132S-3×FLAG* (Isoform 1):**

GCGGCCGCAACTTAAAAAAAAAAATCAAAATGGCCGCCACCGCCCTGCTGGAGGCC

GGACTGGCCCGCGTGCTGTTTTACCCAACCCTGCTGTATACCCTGTTTCGCGGAAAG

GTGCCCGGACGCGCCCACCGCGATTGGTACCACCGCATCGACCCCACCGTGCTGCTG

GGAGCCCTGCCCCTGCGCTCGCTGACCCGCCAGCTGGTGCAGGATGAGAACGTGCG

CGGCGTGATCACCATGAATGAGGAGTACGAGACGCGCTTCCTGTGCAACTCGTCGC

AGGAGTGGAAGCGCCTGGGAGTGGAGCAGCTGCGCCTGAGCACCGTGGATATGACC

GGCATCCCAACCCTGGACAATCTGCAGAAGGGCGTGCAGTTCGCCCTGAAGTACCA

GTCCCTGGGCCAGTGCGTGTACGTGCACAGCAAGGCCGGACGCTCGCGCAGCGCCA

CGATGGTGGCCGCCTACCTGATCCAGGTGCACAAGTGGTCCCCAGAGGAGGCCGTG

CGCGCCATTGCCAAGATCCGCTCGTACATTCACATTCGCCCGGGACAGCTGGATGTG

CTGAAGGAGTTCCACAAGCAGATCACCGCCCGCGCCACCAAGGATGGAACCTTCGT

GATCTCCAAGACC**GACTACAAGGATGACGACGATAAGGATTACAAGGATGACGA**

CGATAAGGACTACAAGGATGACGATGATAAGTGATCTAGA

Mitochondrial enrichment: To generate subcellular fractions enriched for mitochondria, forty 1-3 day-old adult flies (20 male and 20 female or 40 larvae for *Act5C-GAL4 > UAS-ΔMTS-dPTPMT1* flies) were homogenized in 1 ml mitochondrial isolation buffer (MIB: 70 mM sucrose, 210 mM Mannitol, 50 mM Tris/HCl pH 7.5, 10 mM EDTA/Tris pH 7.5) with protease inhibitors (Roche, 04693116001) at 4°C. Lysate was centrifuged twice at 600g for 10 minutes at 4°C to remove cell debris and nuclei. A portion of this lysate was removed for the "whole cell fraction." Samples were subsequently centrifuged at 7,000g for 10 minutes at 4°C to pellet mitochondria.

The mitochondrial pellet was resuspended three times in MIB to wash the pellet and then finally re-suspended in MIB. The supernatant was saved as the "cytosolic fraction". Protein concentration was measured using Pierce^{TM} BCA Protein Assay kit (Thermo Scientific, 23225), according to manufacturer's instructions. Equal total protein from each fraction was (1 μg) was loaded. Mitochondrial enrichment experiments were repeated three times using adults/larvae from independent crosses.

Western blotting: To verify expression of *dPTPMT1* transgenes, *Act5C-GAL4* virgins were crossed to males carrying each transgene. Ten 3rd instar larvae were collected for each genotype and homogenized in 100 μl of RIPA buffer (Thermo Scientific, 89900) with protease inhibitors (1:1000, Millipore Sigma, 539134). Lysates were centrifuged at 17,000g for 20 minutes at 4°C and then diluted 1:8 in Laemmli buffer (BioRad, 1610737) and RIPA. Primary antibodies used include anti-FLAG (Sigma Aldrich, F7425) at 1:1000, anti-Actin (Abcam, ab8224) at 1:3000, anti-Tubulin (Invitrogen, 62204) at 1:3000**,** anti-hPTPMT1 (Thermo Scientific, PA5-60557) at 1:1000, and anti-dMIC60 (Tsai et al., 2018) at 1:6000. Secondary antibodies used include HRP-conjugated goat anti-mouse IgG (Jackson ImmunoResearch, 115035166) and HRP-conjugated goat anti-rabbit IgG (Jackson ImmunoResearch, 111035144) at 1:5000 for chemiluminescent imaging. For representative chemiluminescent images, immunoblots were imaged on an SRX-101A film processor (Konica Minolta).

Quantification of tracheal air filling: To assess tracheal air filling during the 1st to 2nd instar molt, 50-100 virgin females were crossed to 10-30 males in egg laying chambers on plates containing standard sugar-yeast media (SY: 15 g/L agar, 50 g/L sugar, 100 g/L autolysed yeast, 6 g/L nipagin

and 3 mL/L propionic acid) (Kinghorn et al., 2015). Flies were fattened with yeast for 3 days. On the day of collection, females laid for 2 hours on a fresh plate. These embryos were discarded, and a new plate was placed in the chamber. Eggs were collected for 3 hours and then the plates were removed from the chamber and placed back in the incubator at 25ºC. Forty-eight hours AEL, large 1st instar larvae were selected and transferred to individual wells in a 24-well plate filled with SY media at room temperature (22 ºC). Larvae were observed every 30 minutes. The onset of molting was marked by the presence of a double vertical plate (dVP) and was considered complete once the outer cuticle and 1st instar mouthparts were shed (Park et al., 2002). At this timepoint, if the trachea was not filled with air it was counted as having incomplete air filling. Air filling was assessed in the dorsal trunk of the trachea using a transmitted light microscope. Trachea that are filled with air have a silvery appearance that makes the trachea readily visible. For *dPTPMT1*^{mut1} mutants, air filling was assessed in 3rd instar escapers grown in standard molasses media vials. Vials were flipped every 3-4 days. 3rd instar escapers were resuspended in 20% sucrose, washed in distilled water and their trachea were examined under transmitted light for air-filling defects in the dorsal trunk of the trachea. Each experiment was repeated a minimum of 2 times using independent crosses.

Quantification of tracheal blackening: For quantification of tracheal blackening in adults with ubiquitous *dPTPMT1* RNAi, parents laid eggs for 3 days at 25ºC after which their progeny were transferred to 30ºC for the remainder of development. Adult males were assessed for tracheal blackening 0-2 days post-eclosion. For assessments of the strength of tracheal blackening in adults, we used the following scale. Adults were scored as “none” if they had no visibly blackened trachea, “weak” if they had light blackening in one tracheal region, “moderate” if they had one heavily

blackened tracheal region or multiple light to moderately blackened regions, and "strong" if they had multiple heavily blackened tracheal regions. For assessment of tracheal blackening in adults with ubiquitous expression of *hPTPMT1* in a wild-type background, equal number of males and females were assessed 0-2 days after eclosion. For assessments of tracheal blackening in 3rd instars with ubiquitous *dPTPMT1* RNAi, parents were allowed to lay for 24 hours and then removed from the vial. Vials were transferred to 30°C. Once 3rd instar larvae were visible on the side of the vial, larvae were re-suspended in 20% sucrose and washed briefly in phosphate buffered saline (PBS) in preparation for assessment. For assessment of tracheal blackening in 2nd instars with *btl-GAL4*-driven RNAi of *dPTPMT1* see "Viability Assays" below. For assessment of tracheal blackening in $dPTPMT1^{mut1}$ 3rd instar escapers, crosses were grown at 25°C and flipped once every three days. 3rd instar escapers were resuspended following the criteria for larvae outlined above. For assessment of the strength of tracheal blackening in larvae, we used the following scale. Larvae were scored as "strong" if more than 50% of the dorsal trunk of the trachea was blackened, "moderate" if less than 50% but greater than 10% of the dorsal trunk of the trachea was blackened, "weak" if less than 10% of the dorsal trunk of the trachea was blackened, and "none" if they had no visible tracheal blackening. For tracheal-specific RNAi experiments, decomposed larvae were omitted from the assessment and categorized as "can't tell". Each experiment was repeated a minimum of 2 times using independent crosses.

Survival assays: For survival assays with *Act5C-GAL4* RNAi (Figure 1D), 3 independent crosses were set up at 25°C. After 3 days, parents were removed from the vial and the remaining progeny were transferred to 30°C. 3rd instar larvae were floated out of the media with 20% sucrose, washed in PBS, and then transferred to fresh vials. Three replicates (1 vial per independent cross) of 25-

26 3rd instar male larvae per vial were performed for RNAi 1& 2 and its background control. Six replicates (2 per independent cross) with 4-25 3rd instar male larvae per vial were performed for RNAi 3 and its control. The percentage of 3rd instars surviving to pupal stage and adult stage was determined.

Viability assays: For early larval viability assays with CRISPR mutants (Figure 1B), eggs were collected for 3 hours following the methods described above, see "Quantification of tracheal air filling". Twenty-four hours AEL, the number of viable and non-viable 1st instar larvae were counted to assess early survival in *dPTPMT1*^{mut1} mutants. If a larva did not respond to mechanical stimulus it was counted as non-viable. This assay was repeated three times using independent crosses. For viability experiments with *btl-GAL4* RNAi (Figure 2E), eggs were collected for 3 hours following the methods described above. 1st instar larvae were collected 24 hours AEL and placed in vials containing SY media for the continuation of development. Larvae were floated out of the media with 20% sucrose and then poured out onto filter paper for assessment. Larvae were assayed cross-sectionally for viability at 48 hours, 72 hours, 96 hours, and 120 hours post-egg collection. If a larva did not respond to mechanical stimulus it was counted as non-viable. The percentage of viable larvae in each vial was determined at each time point. Larvae were also assessed for tracheal blackening and developmental stage at 48 hours, 72 hours, and 96 hours. Assays were repeated 2-3 times using independent crosses with 2-4 vials per cross, with 13-30 larvae per vial. To quantify adult viability (Figure 1C, 4I, and S4C), the number of adults of each genotype was counted within 0-2 days of eclosion. Genotypic frequency was calculated and then normalized to the expected genotypic frequency for that genotype. In cases where the genotype of interest had a viability of above 100%, the siblings of this genotype (for example, *UAS-*

RNAi/*TM3*(*ActGFP*, *ser*)) showed slight reductions in viability, which is to be expected given the multiple inversions present within balancer chromosomes. For these assays, tracheal blackening was also assessed in all adults, 0-2 days post-eclosion. A minimum of three independent crosses were quantified for each genotype.

ATP assay: ATP levels were measured using a luciferase-based bioluminescence assay (ATP Bioluminescence Assay Kit HS II, 11699709001, Roche Applied Science) following manufacturer's instructions. For each measurement, a single fly was homogenized in 100 µl of lysis buffer (provided by the kit). The lysate was boiled for 5 minutes, briefly placed on ice, and then cleared by centrifugation at 17,000g for 1 minute. Lysates were diluted 1:50 with dilution buffer (provided by the kit) and then incubated with equal volume of luciferase. Luminescence was immediately measured using a FlexStation 3 (Molecular Devices). A minimum of 7 replicates were performed for each genotype. Values were normalized to total protein, as measured by the BCA assay.

Sample preparation for imaging and data analysis: Stereoscopic images of adults and larvae were taken using a DEM130 Digital Eyepiece (2M pixels CMOS) or a Leica S9i (Leica Microsystems). Fluorescence patterns in *Drs-GFP* flies were assessed using a SMT1-FL Fluorescence Stereo-Microscope System (Tritech Research). Adult flies were anesthetized using an ice pack during assessment. If fluorescence was observed in the inner tracheal tube of the leg, the fly was counted as having *Drs-GFP* expression in the trachea. For *Drs-GFP* examination of adults, females were assessed because males had reduced viability on this background. Flies were assessed at the same time of day to control for circadian variation in immune gene expression

(Neyen et al., 2014). *Drs-GFP* flies were imaged using a Leica M165 FC (Leica Microsystems). Flies were anesthetized using dry ice during imaging. Confocal imaging was performed using a Leica SPE laser scanning confocal microscope (Leica Microsystems). For live-imaging of mito-GFP**,** 1st and 2nd instar larvae were collected using the methods described above, see "Quantification of tracheal air filling". Larvae were immobilized beneath a piece of clear tape and assessed for the presence of mito-GFP puncta within the dorsal trunk and tracheal branches. A posterior region of the dorsal trunk of the trachea was then selected for imaging. For *in vivo* ROS detection, *mito-roGFP2-Orp1* and *Grx1* were used to measure mitochondrial ROS levels in the trachea of intact larvae. *UAS-mito-roGFP2-Orp1* or *Grx1* were expressed in fly trachea using the *btl-GAL4* driver. 1st and 2nd instar larvae were collected and mounted using the methods described for mito-GFP. Larvae were imaged following the methods of Albrecht and colleagues (Albrecht et al., 2011, Barata and Dick, 2013). Specifically, excitation of roGFPs by the 405nm and 488nm laser was performed sequentially. Emission was detected at 500-530nm. This system was calibrated using dissected tracheal tissue treated with 10mM dithiothreitol or 1mM diamide, to produce fully reduced or oxidized samples, respectively. For processing, images were converted to a 32-bit format. Following background subtraction, the 488 nm image was thresholded and pixels outside of the threshold were converted to "NaN." Ratios were calculated by dividing the pixel intensity of the 405 nm image by the 488 nm image. For TUNEL staining, tracheae were dissected in PBS, fixed with 4% paraformaldehyde for 20 minutes at room temperature, and then washed with PBS. Tracheae were permeabilized for 20 minutes at room temperature with 0.6% (vol/vol) Triton-100 and 0.6% (wt/vol) sodium deoxycholate, and then washed with PBS. After permeabilization, the protocol outlined in the In Situ Cell Death Detection Kit (12156792910, Sigma/Roche) was followed. Tracheae were cover-slipped with ProLong™ Glass Antifade

Mountant with NucBlue™ Stain (Thermo Fisher, P36981) and cured at room temperature (22°C) for 48-60 hours, following the manufacturer's recommendations. All fluorescent images were adjusted for brightness.

Transmission electron microscopy: For TEM, 3rd instar male larvae were filleted in 1 × Ca^{2+} free saline (0.128 M NaCl, 2 mM KCl, 5 mM EGTA, 4 mM $MgCl_2$, 5 mM HEPES, 0.0355 M sucrose), and fixed in Karnovsky's fixative (0.1 M sodium cacodylate buffer pH 7.4, 2% glutaraldehyde, and 4% paraformaldehyde) at room temperature (22°C, RT) for 30 minutes and then kept at 4°C overnight. Specimens were post-fixed in cold/aqueous 1% osmium tetroxide for 1 hour, warmed to RT for 2 hours, and then rinsed 3 times in ultra-filtered H_2O. Specimens were subsequently stained en bloc with 1% uranyl acetate at RT for 2 hours, dehydrated in a graded ethanol series, immersed in propylene oxide (PO) for 15 minutes, infiltrated with a graded series of PO and Embed-812 resin, and then embedded in EMbed-812 resin at 65°C overnight. Specimens were sectioned transversely at segment A1/A2 or in the case of the *btl-GAL4 > UAS-dPTPMT1* RNAi larva, in a region where tracheal blackening was visible. Sections were cut to a thickness of 75-90 nm and laid on formvar/carbon-coated slot Cu grids. Sections were stained for 40 seconds with 3.5% uranyl acetate in 50% acetone followed by Sato's Lead Citrate for 2 minutes. Sections were observed using a JEM-1400 120kV (Joel, Japan) and images were taken using an Orius 832 4k X 2.6k digital camera with 9um pixel (Gatan, CA). Images were processed with Photoshop CS6. Tracheal tubes were identified by their unique structure (i.e. a simple epithelial monolayer, with a lumen and an internal tracheal cuticle).

Statistical analyses: Throughout this paper, the distribution of data points is expressed as mean ± SEM, unless otherwise stated. Individual data points are shown in bar graphs where $n \leq 6$. For roGFP experiments, data is displayed as box-and-whiskers, as is conventional for these experiments (Albrecht et al., 2011). Boxes show $25^{th}/75^{th}$ percentiles, whiskers are the minimum and maximum values, and x is the median marker. For comparisons between two groups, F-test was performed, followed by t-test. Chi-square test was used to determine statistical significance for groups of categorical data. The number of flies and experimental replicates (n) are in figure legends and methods. *: $p < 0.05$, **: $p < 0.01$, ***: $p < 0.001$. Statistical experiments were performed in Excel or GraphPad Prism 8 Software.

SUPPLEMENTAL REFERENCES

GROTH, A. C., FISH, M., NUSSE, R. & CALOS, M. P. 2004. Construction of transgenic Drosophila by using the site-specific integrase from phage φC31. *Genetics,* 166**,** 1775-1782.

KINGHORN, K. J., CASTILLO-QUAN, J. I., BARTOLOME, F., ANGELOVA, P. R., LI, L., POPE, S., COCHEMÉ, H. M., KHAN, S., ASGHARI, S., BHATIA, K. P., HARDY, J., ABRAMOV, A. Y. & PARTRIDGE, L. 2015. Loss of PLA2G6 leads to elevated mitochondrial lipid peroxidation and mitochondrial dysfunction. *Brain,* 138**,** 1801-1816.

LIVAK, K. J. & SCHMITTGEN, T. D. 2001. Analysis of relative gene expression data using real-time quantitative PCR and the 2^{-} ΔΔCT method. *methods,* 25**,** 402-408.

NEYEN, C., BRETSCHER, A. J., BINGGELI, O. & LEMAITRE, B. 2014. Methods to study Drosophila immunity. *Methods,* 68**,** 116-128.

PFEIFFER, B. D., TRUMAN, J. W. & RUBIN, G. M. 2012. Using translational enhancers to increase transgene expression in Drosophila. *Proceedings of the National Academy of Sciences,* 109**,** 6626-6631.